Cell Reports

Article

Neonatal diabetes mutations disrupt a chromatin pioneering function that activates the human insulin gene

Graphical abstract

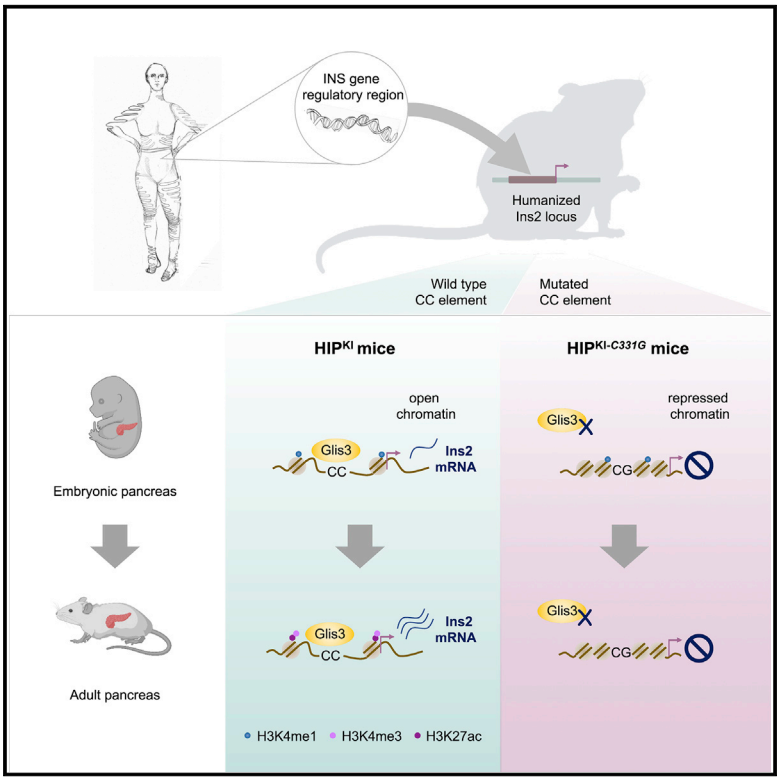

Highlights

- Mutations of a CC dinucleotide in the human *INS* promoter cause neonatal diabetes
- We humanized ~3.1 kb of mouse *Ins2* and created a CC mutant version
- Humanized *Ins2*, but not the CC mutant, recapitulates developmental chromatin activation
- *GLIS3*, also mutated in diabetes, activates *INS* chromatin and requires an intact CC

Authors

Ildem Akerman, Miguel Angel Maestro, Elisa De Franco, ..., Sian Ellard, Andrew T. Hattersley, Jorge Ferrer

Correspondence

i.akerman@bham.ac.uk (I.A.),
jorge.ferrer@crg.eu (J.F.)

In brief

Mutations in the CC element of the *INS* promoter or the transcription factor *GLIS3* cause neonatal diabetes. Akerman et al. humanize a 3.1-kb region upstream of the mouse *Ins2* gene and show that GLIS3 and the CC element form a pioneering mechanism that activates *INS* chromatin during pancreas development.

Akerman et al., 2021, Cell Reports *35*, 108981
April 13, 2021
https://doi.org/10.1016/j.celrep.2021.108981

CellPress

Cell Reports

CellPress
OPEN ACCESS

Article

Neonatal diabetes mutations disrupt a chromatin pioneering function that activates the human insulin gene

Ildem Akerman,[1,2,11,*] Miguel Angel Maestro,[3,4] Elisa De Franco,[5] Vanessa Grau,[3,4] Sarah Flanagan,[5] Javier García-Hurtado,[3,4] Gerhard Mittler,[6] Philippe Ravassard,[7] Lorenzo Piemonti,[8] Sian Ellard,[5,9] Andrew T. Hattersley,[5] and Jorge Ferrer[3,4,10,*]

[1]Institute of Metabolism and Systems Research (IMSR), Medical School, University of Birmingham, Birmingham, UK
[2]Centre for Endocrinology, Diabetes and Metabolism (CEDAM), University of Birmingham, Birmingham, UK
[3]Centre for Genomic Regulation (CRG), The Barcelona Institute of Science and Technology, Dr. Aiguader 88, Barcelona 08003, Spain
[4]Centro de Investigación Biomédica en red Diabetes y Enfermedades Metabólicas Asociadas (CIBERDEM), Barcelona, Spain
[5]Institute of Biomedical and Clinical Science, University of Exeter Medical School, Exeter, UK
[6]Max-Planck Institute for Immunobiology and Epigenetics, Freiburg, Germany
[7]INSERM, CNRS, Paris Brain Institute - Hôpital Pitié-Salpêtrière, Paris, France
[8]Diabetes Research Institute, IRCCS Ospedale San Raffaele and Università Vita-Salute San Raffaele, Milan, Italy
[9]Exeter Genomics Laboratory, Royal Devon and Exeter NHS Foundation Trust, Exeter, UK
[10]Section of Genetics and Genomics, Department of Metabolism, Digestion and Reproduction, Imperial College London, London, UK
[11]Lead contact
*Correspondence: i.akerman@bham.ac.uk (I.A.), jorge.ferrer@crg.eu (J.F.)
https://doi.org/10.1016/j.celrep.2021.108981

SUMMARY

Despite the central role of chromosomal context in gene transcription, human noncoding DNA variants are generally studied outside of their genomic location. This limits our understanding of disease-causing regulatory variants. *INS* promoter mutations cause recessive neonatal diabetes. We show that all INS promoter point mutations in 60 patients disrupt a CC dinucleotide, whereas none affect other elements important for episomal promoter function. To model CC mutations, we humanized an ~3.1-kb region of the mouse *Ins2* gene. This recapitulated developmental chromatin states and cell-specific transcription. A CC mutant allele, however, abrogated active chromatin formation during pancreas development. A search for transcription factors acting through this element revealed that another neonatal diabetes gene product, GLIS3, has a pioneer-like ability to derepress *INS* chromatin, which is hampered by the CC mutation. Our *in vivo* analysis, therefore, connects two human genetic defects in an essential mechanism for developmental activation of the *INS* gene.

INTRODUCTION

Most sequence variants underlying Mendelian diseases affect coding sequences, although several patients are known to harbor causal *cis*-regulatory mutations (Benko et al., 2009; Garin et al., 2010; Hansen et al., 2002; Lettice et al., 2003; Weedon et al., 2014). This number is expected to rise as millions of human genomes are sequenced and the field learns to discriminate pathogenic noncoding mutations from a vast number of inconsequential variants (Chong et al., 2015; Huang et al., 2017; Kowalski et al., 2019; Ward and Kellis, 2012). In polygenic diseases, common and rare *cis*-regulatory variants play a central role in the genetic susceptibility (Cowper-Sal lari et al., 2012; Maurano et al., 2012; Pasquali et al., 2014).

Despite the relevance of *cis*-regulatory variants, they have been largely studied outside their chromosomal context. Current experimental models usually test noncoding variants with episomal DNA constructs, ectopically located transgenes, or *in vitro* protein-DNA interaction assays. The extent to which these models reflect the true impact of *cis*-regulatory variants is unknown. Expression quantitative trait loci can provide insights into which genes are affected by regulatory variants in their native genome context yet often fail to distinguish causal from linked variants. It is now also possible to directly edit mutations in stem cells and differentiate them *in vitro*, but this does not always allow modeling the mutational impact in relevant developmental or physiological *in vivo* contexts. There is a need, therefore, to develop complementary tools that facilitate understanding of the *in vivo* impact of noncoding variants.

One approach to address this need is to engineer human genomic sequences in mice. Several examples of human knock-ins in the mouse genome have been created to model human protein-coding mutations (Zhu et al., 2019). One study successfully edited a 5-bp noncoding sequence in mice to model a common human regulatory variant (Pashos et al., 2017). However, the extent to which mice can be used to study human *cis*-regulatory mutations in more-extended orthologous genomic contexts is poorly explored.

Modeling noncoding mutations in model organisms poses major challenges, because the consequence of mutations that disrupt transcription factor-DNA interactions can be influenced by essential combinatorial interactions with nearby transcription factor binding sites or by the existence of redundant binding sites (Biggin, 2011; Heinz et al., 2013; Junion et al., 2012). Unlike coding sequences, which are often highly conserved, noncoding DNA sequences can maintain functions despite substantial evolutionary turnover, and conserved noncoding sequences can acquire divergent functions (Khoueiry et al., 2017; Villar et al., 2015). It is thus difficult to predict pathological consequences of human *cis*-regulatory mutations from mouse models unless the broader sequence context has been humanized.

We have now examined a *cis*-regulatory mutation in the *INS* gene that causes diabetes mellitus. A subset of patients with neonatal diabetes harbors recessive loss-of-function coding or promoter mutations in *INS*, encoding for insulin (Garin et al., 2010). Single-nucleotide mutations of the INS promoter published so far are located in a CC dinucleotide 331 bp upstream of the *INS* start codon (Bonnefond et al., 2011; Deeb et al., 2016; Demirbilek et al., 2015; Garin et al., 2010). Functional studies in tumoral β cells using episomal luciferase assays showed that c.-331C > G, the most common of these mutations, causes partial disruption of *INS* promoter activity (Garin et al., 2010). However, decades of work have shown that artificial mutations in various other elements of the *INS* 5′ flanking region that disrupt binding by transcription factors, such as MAFA, PDX1, or NEUROD1, also lead to reduced transcriptional activity in episomal assays (Docherty et al., 2005; German et al., 1995; Le Lay and Stein, 2006; Melloul et al., 2002; Odagiri et al., 1996). This raises the question of whether the CC element is specifically vulnerable due to an essential role in the *in vivo* regulation of the *INS* gene that cannot be examined in episomal assays.

In this study, we establish the selectivity of CC element mutations in an extended cohort of patients. We humanized a large noncoding region of the mouse *Ins2* gene and used a mutant version of this model to show that the c.-331C > G mutation disrupts active chromatin formation during pancreas development. We then linked the CC element to GLIS3, a zinc finger transcription factor that also carries neonatal diabetes mutations, as well as type 1 and type 2 diabetes risk variants (Barrett et al., 2009; Dupuis et al., 2010; Senée et al., 2006). GLIS3, one of several transcription factors known to regulate the insulin gene (Kang et al., 2009; Yang et al., 2009), showed a singular capacity to create *INS* gene active chromatin in non-pancreatic cells, and this was inhibited in the CC mutant. This *in vivo* analysis of two regulatory defects has therefore revealed a pioneering mechanism of the human *INS* gene. These insights are relevant to the mechanisms of diabetes and for regenerative strategies that aim to activate the *INS* gene in non-pancreatic cells.

RESULTS

Human genetics establishes a unique role of the *INS* promoter CC element

To further define the importance of the *INS* promoter CC element, we re-examined the selectivity of mutations in a large cohort of previously published (n = 19) and unpublished (n = 41) patients with diabetes caused by recessive *INS* promoter mutations. This showed that, among 60 patients from 44 families, all single-base-pair mutations located 5′ of the transcriptional start site resided in the CC element. This included 42 patients with c.-331C > G mutations (40 homozygous; two compounds heterozygous), two with c.-332C > G mutations (one homozygous; another compound heterozygous), and 13 with c.-331C > A mutations (12 homozygous; one compound heterozygous with a c.-331C deletion; Figure 1; Table S1). This newly described c.-331C single-base-pair deletion is interesting, because it strongly favors a loss- rather than gain-of-function mechanism for CC mutations. The only other pathogenic *INS* upstream mutation was a larger homozygous deletion that disrupts MAFA and NEUROD1 binding sites, which was observed in four patients from two families. Most patients had characteristic clinical features of insulin-deficient neonatal diabetes, with low birth

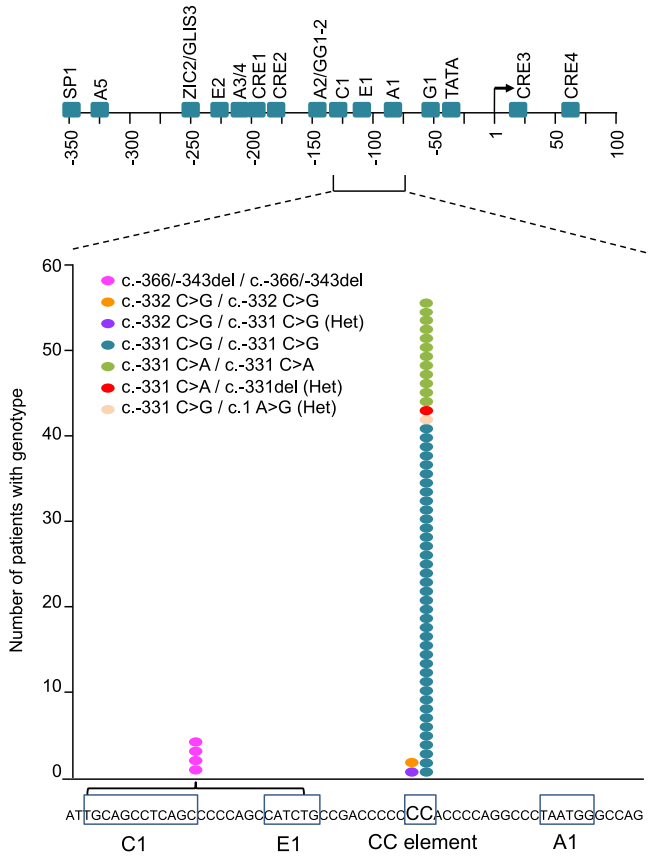

Figure 1. Location of *INS* promoter mutations

The top panel is a schematic of the human *INS* 5′ flanking sequence, showing approximate locations of established *cis*-regulatory sequences based on published mutational analyses of episomal sequences. The bottom panel shows a zoomed-in sequence that contains previously characterized MAFA, NEUROD1, and PDX1-bound *cis*-elements (C1, E1, and A1, respectively), as well as the CC element, with a graph that depicts the location of all *INS* promoter recessive mutations from our analysis. Each dot represents a patient, and the color represents the genotype. All single-base-pair mutations are located in the CC element, including a distinct 24-bp deletion that disrupts MAFA and NEUROD1 binding sites.

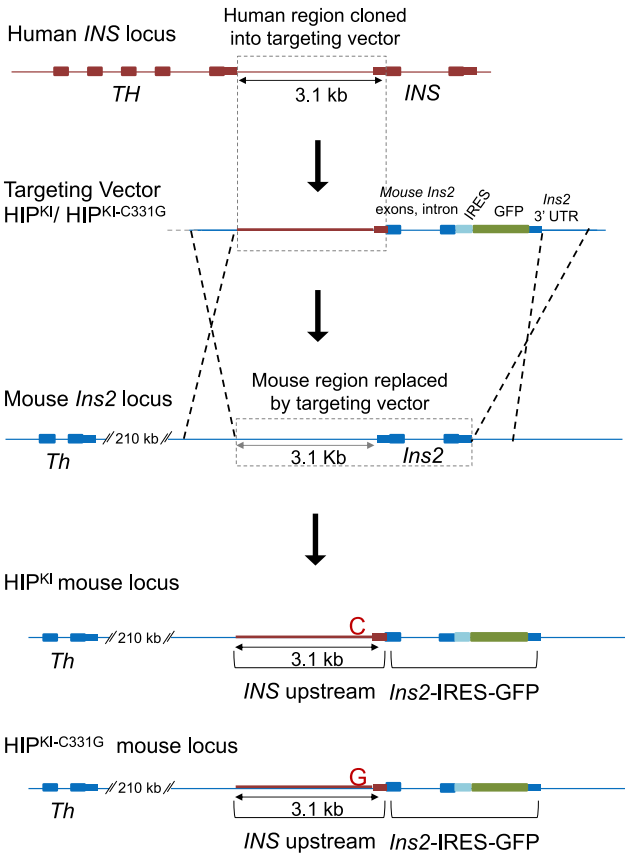

Figure 2. Generation of HIP^{KI} and HIP$^{KI\text{-}C331G}$ mouse alleles

A rectangle with dotted lines in the top two panels depicts the 3.1-kb human sequence located between the human *TH* and *INS* genes (including *INS* 5′ untranslated transcribed sequences), which was cloned into a targeting vector. This targeting vector contained the 3.1-kb human INS upstream region followed by Ins2-IRES-GFP, which includes mouse *Ins2* exons and intron and an IRES, GFP, and *Ins2* 3′ UTR and was flanked by mouse *Ins2* homology arms. Targeted replacement of the indicated mouse *Ins2* sequence with this human upstream *INS* sequence followed by Ins2-IRES-GFP was carried out by homologous recombination. The same process was used to create two allelic versions carrying the normal human *INS* sequence or the c.-331C > G mutation. A neomycin cassette flanked by LoxP sites was excised *in vivo* and is omitted for simplicity. The sequence of the neomycin-excised targeted allele is provided in File S1.

weight and diabetes onset soon after birth, although 2 patients were diagnosed outside the neonatal period and 12 (including both patients with -332 mutations) showed transient neonatal diabetes (Table S1). No associated clinical abnormalities were consistently noted in this patient series. These extended human genetic findings, therefore, establish that the CC dinucleotide sequence of the *INS* promoter is unusually sensitive to mutations, suggesting a singular function of this *cis*-regulatory element.

Generation of a human *cis*-regulatory mutation mouse model

To study the function of the CC element *in vivo*, we modeled the c.-331C > G mutation in a humanized sequence context. We generated mice in which homologous recombination was used to replace the endogenous 3.17-kb mouse genomic region containing the *Ins2* gene and its upstream regions with a human *INS* upstream DNA fragment. This genomic region showed high-sequence conservation to the mouse counterpart in an ~350-bp region upstream of *INS* TSS and another ~500-bp region downstream of the *TH* gene but contained intervening sequences lacking identifiable orthology with the mouse genome, including a primate-specific variable number tandem repeat region previously reported to influence *INS* transcription (Kennedy et al., 1995; Figure S1A). The knocked in allele thus contained (1) this 3.10-kb upstream region of human *INS*, including a transcribed *INS* 5′ untranslated sequence; (2) mouse *Ins2* exon1, intron, and exon 2; and (3) an internal ribosome entry site (IRES) followed by green fluorescent protein (GFP) sequence (Figure 2). The resulting transcript was thus translated into two proteins: mouse preproinsulin-2 and GFP. In parallel, we generated a mouse model harboring the same humanized sequence and the *INS* c.-331C > G single point mutation (Figure 2). We named mice carrying the two human *INS* upstream knockin alleles HIP^{KI} and HIP$^{KI\text{-}C331G}$.

Homozygous HIP^{KI} and HIP$^{KI\text{-}C331G}$ mice were born at expected Mendelian ratios and appeared healthy without overt hyperglycemia (Figure S1B), consistent with the fact that HIP knockin mice retained an intact copy of *Ins1*, a retroposed mouse gene that also encodes insulin (Duvillié et al., 1997; Leroux et al., 2001).

HIP^{KI} recapitulates, and HIP$^{KI\text{-}C331G}$ abrogates, cell-specific *INS* transcription

To determine whether the human *INS* 5′ flanking region inserted into its orthologous mouse chromosomal context was able to drive β-cell-specific expression in HIP^{KI} mice, we used dual immunofluorescence analysis of GFP and islet hormones in tissues from newborn mice (postnatal day 1 [P1]–P3). This showed that GFP expression was restricted to insulin-positive pancreatic islet core β cells of HIP^{KI} mice, whereas it was not detected in mantle glucagon- or somatostatin-positive islet cells or surrounding exocrine cells (Figures 3A and 3B). Moreover, GFP fluorescence was readily detected in live islets isolated from 3- to 5-month-old HIP^{KI} mice (Figure 3C). *Ins2-IRES-GFP* transcript was also restricted to islets across a panel of mouse tissues (Figure S1C).

In sharp contrast to HIP^{KI} islets, HIP$^{KI\text{-}C331G}$ islets showed no detectable GFP fluorescence or immunoreactivity (Figures 3A–3C). Thus, *Ins2-IRES-GFP* expression in HIP^{KI} mice recapitulates expected β-cell-specific patterns of insulin expression, whereas the HIP$^{KI\text{-}C331G}$ mutation disrupts this expression pattern.

To further assess the function of human *INS* flanking regions, we measured *Ins2* mRNA in islets isolated from HIP^{KI} and HIP$^{KI\text{-}C331G}$ mice. Quantitative RT-PCR analysis revealed *Ins2* mRNA in islets isolated from both control C57BL/6 and HIP^{KI} mice, but not in HIP$^{KI\text{-}C331G}$ mouse (Figure 3D), thus confirming that the c.-331C > G single point mutation abrogates transcriptional activity of the humanized *INS*/*Ins2* locus in mice. We note, however, that *Ins2* transcripts in HIP^{KI} islets, which form part of the larger *Ins2-IRES-GFP* transcript, were reduced in comparison to control C57BL/6 islets (Figure 3C).

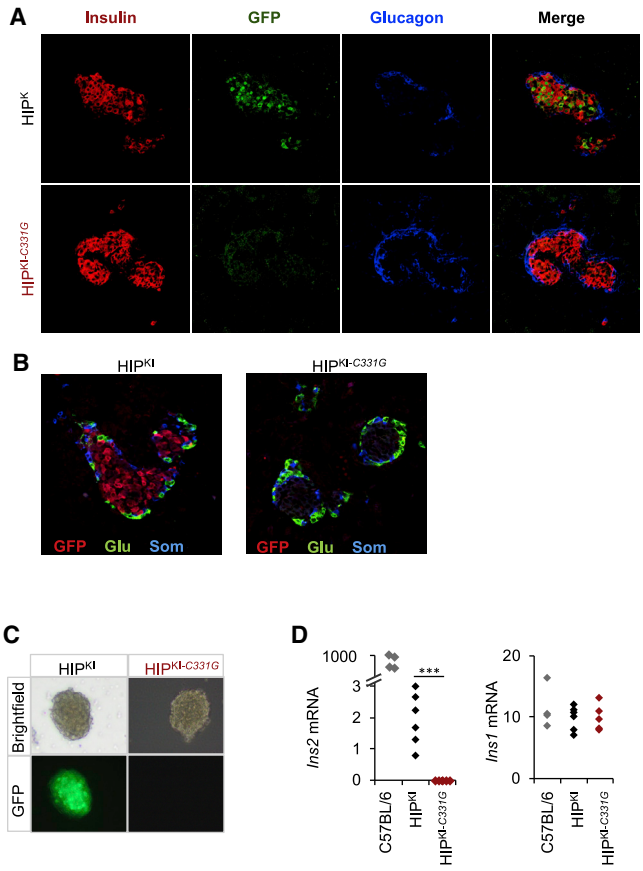

Figure 3. HIP^{KI} recapitulates and HIP$^{KI\text{-}C331G}$ abrogates β cell-specific *Ins2* expression

(A) Immunofluorescence imaging of insulin, glucagon, and GFP, showing selective GFP expression in HIP^{KI} insulin-positive core islet cells, but not in the surrounding glucagon islet mantle, or in extra-islet exocrine cells. In contrast, no GFP expression is detected in HIP$^{KI\text{-}C331G}$ islet cells.

(B) Immunofluorescence imaging of glucagon, somatostatin, and GFP, showing lack of GFP expression in somatostatin or glucagon-positive cells.

(C) Bright-field and fluorescence imaging of islets isolated from HIP^{KI} and HIP$^{KI\text{-}C331G}$ mice.

(D) Quantitative PCR analysis of *Ins2* and *Ins1* mRNAs in pancreatic islets from 3- to 5-month-old C57BL/6 (n = 4), HIP^{KI} (n = 6), and HIP$^{KI\text{-}C331G}$ (n = 6) mice. Values were normalized to *Actb* mRNA. ***p < 0.0001 (Student's t test).

This resulted from a combined effect of ~10-fold reduced transcription and ~14-fold reduced stability of the *Ins2-IRES-GFP* transcript, as compared to the intact *Ins2* mRNA from C57BL/6 islets (Figures S1D and S1E).

Further analysis revealed normal levels of *Ins1*, *Pdx1*, *Glis3*, *NeuroD1*, *MafA*, *Glut2*, and *Gck* mRNAs in HIP^{KI} and HIP$^{KI\text{-}C331G}$ islets, suggesting that humanization of regulatory sequences in the mouse *Ins2* locus did not impact these key pancreatic β cell identity markers (Figures 3C and S1F).

Mice with homozygous null *Ins2* mutations display mild transient hyperglycemia (Duvillié et al., 1997; Leroux et al., 2001). Consistently, HIP$^{KI\text{-}C331G}$ mice, which were *Ins2*-deficient, showed mildly increased glycemia (119[32] versus 145[24] mg/dL; mean [IQR]; Student's t test p = 0.0031; Figure S1A).

These findings indicate that an ~3-kb human *INS* upstream region can replace its mouse orthologous region and still direct cell-specific transcription in mouse β cells. Furthermore, they show that the human *INS* c.-331C > G point mutation abrogates the function of this humanized region, consistent with the severe phenotype observed in humans with neonatal diabetes.

HIP^{KI}, but not HIP$^{KI\text{-}C331G}$, islets mirror human islet *INS* chromatin

Nucleosomes that flank promoters of transcriptionally active genes are typically enriched in trimethylated histone H3 lysine 4 (H3K4me3) and acetylated histone H3 lysine 27 (H3K27ac), and this was expectedly also observed in the human *INS* promoter in human islets (Morán et al., 2012; Pasquali et al., 2014; Figure S2). We thus examined these histone modifications at the *INS* promoter in HIP^{KI} and HIP$^{KI\text{-}C331G}$ adult mouse islets by chromatin immunoprecipitation (ChIP) assays. The *INS* proximal promoter showed enriched H3K4me3 and H3K27ac in adult HIP^{KI} mouse islets (Figures 4A–4C). By contrast, HIP$^{KI\text{-}C331G}$ islets showed 5-fold and 7-fold lower signals (Student's t test; p < 0.001; Figures 4B and 4C). HIP$^{KI\text{-}C331G}$ islets also showed markedly reduced *INS* promoter chromatin accessibility as measured by formaldehyde-assisted isolation of regulatory elements (FAIRE) (Figure 4D) and reduced binding of PDX1, an islet transcription factor that binds to multiple sites in the *INS* promoter (Figure 4E). These findings, therefore, demonstrate that the c.-331C > G point mutation does not only prevent transcriptional activity conferred by the human *INS* 5′ flanking region but also the formation of accessible active chromatin and thereby occupancy by a key *INS* gene transcription factor.

Activation of humanized *INS* locus during development

We next used HIP^{KI} and HIP$^{KI\text{-}C331G}$ models to assess how the c.-331C > G mutation influences chromatin activation at the *INS* gene during pancreas development. As a reference, we analyzed ChIP sequencing (ChIP-seq) maps of H3K4me1 and H3K4me3 histone modifications in human fetal pancreas at Carnegie stage 23 (Cebola et al., 2015), which precedes *INS* gene activation, and compared them with analogous maps from adult human islets (Morán et al., 2012; Pasquali et al., 2014). In the human fetal pancreas, we observed that the histone modification H3K4me1 demarcated a broad region that encompasses the *TH* and *INS* genes as well as downstream regions, without detectable H3K4me3, a histone modification associated with active promoters (Figure 5A). This combination, H3K4me1 enrichment and absence of H3K4me3, has been described in genomic regions that are poised for gene activation (Creyghton et al., 2010) and is consistent with the virtual absence of *INS* transcription in the early fetal pancreas. In adult human islets, by contrast, H3K4me1 in the *INS* locus was largely replaced with H3K4me3, in keeping with active *INS* transcription (Figure 5A).

We next examined whether the chromatin environment that precedes transcriptional activation of the *INS* locus is recapitulated in HIP^{KI} embryos. As in human fetal pancreas, we observed deposition of H3K4me1 in the humanized *INS* flanking regions in HIP^{KI} embryonic day 12.5 (E12.5) mouse fetal pancreas (Figure 5B). *Ins2* mRNA was expectedly not detected above background levels at this stage (Figure 5C). Interestingly, both HIP^{KI}

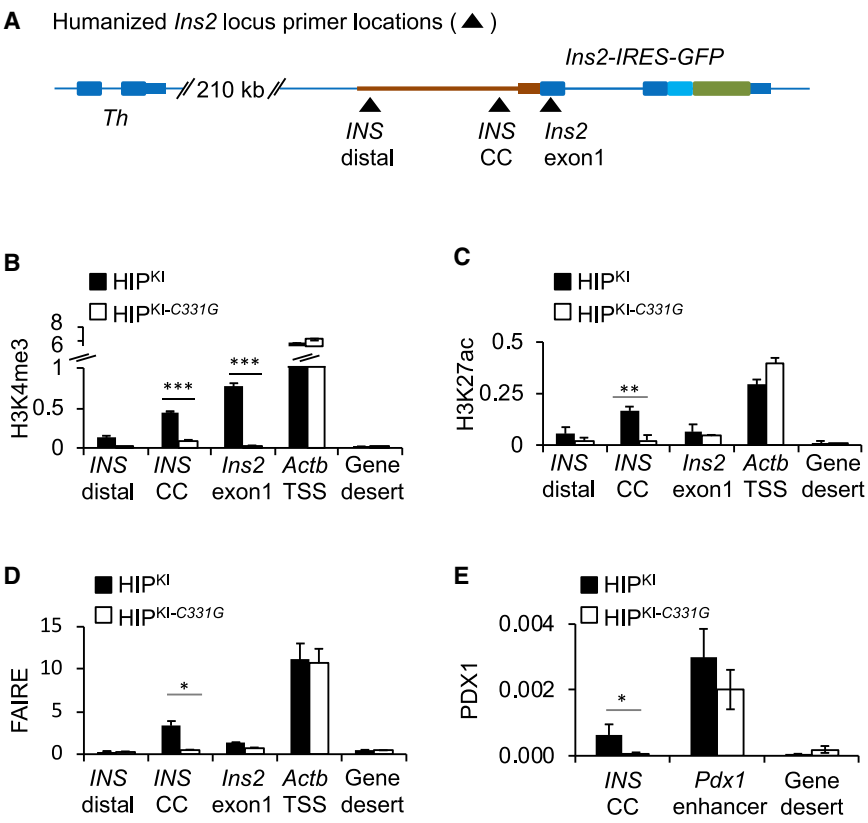

Figure 4. HIP^{KI} recapitulates and HIP$^{KI\text{-}C331G}$ abrogates formation of active chromatin at the *INS* locus

(A) Schematic showing approximate primer locations for ChIP assays. *INS* CC primers encompass the CC element.

(B–D) ChIP quantification of H3K4me3, H3K27ac, and FAIRE accessibility at the humanized *INS* locus and control regions in HIP^{KI} or HIP$^{KI\text{-}C331G}$ adult mouse islets. The *Actb* promoter was used as a positive control, and a gene desert lacking active histone modifications in islets was used as a negative control. ChIP and FAIRE DNA were expressed as a percentage of the total input DNA. n = 3 independent experiments.

(E) ChIP for the transcription factor PDX1 in HIP^{KI} or HIP$^{KI\text{-}C331G}$ adult mouse islets at a known PDX1-bound enhancer near *Pdx1* as a positive control. Data are expressed as a percentage of input DNA. n = 3 independent experiments. Error bars indicate SEM; asterisks indicate Student's t test p values (*p < 0.05; **p < 0.001; ***p < 0.0001).

and HIP$^{KI\text{-}C331G}$ displayed similar H3K4me1 profiles at E12.5 (Figure 5B), indicating that the humanized *INS* sequences recapitulate poised chromatin preceding gene activity, and this is not impeded by the c.-331C > G mutation.

By contrast, the c.-331C > G mutation prevented the transcriptional activation of the humanized locus at early stages of β cell differentiation. Thus, *Ins2* mRNA was detectable in *HIP*^{KI} E15.5 fetal pancreas, but it was undetectable in HIP$^{KI\text{-}C331G}$ embryos (Figure 5C), whereas *Ins1* mRNA was readily detected in both HIP^{KI} and HIP$^{KI\text{-}C331G}$ E15.5 pancreas (Figure 5C). Thus, mice carrying humanized regulatory regions in the *Ins2* locus can recapitulate salient developmental features of the chromatin landscape of the human *INS* locus and show that, although the c.-331C > G mutation does not affect *INS* chromatin poising, it disrupts activation of promoter chromatin in differentiated cells.

GLIS3-dependent activation of the *INS* gene is prevented by c.-331C > G

We next sought to identify factors whose DNA binding activity is influenced by the c.-331C > G mutation. We performed stable isotope labeling by amino acids in cell culture (SILAC) experiments and identified four zinc finger transcription factors (MAZ, ZFP37, KLF13, and KLF16) that showed decreased *in vitro* binding to the c.-331C > G mutation and additionally selected 5 zinc finger transcription factors expressed in human islets that were predicted to show differential binding based on *in silico* and/or literature analysis (Figure S3A). Of these 9 candidate transcription factors, GLIS3, which was previously shown to bind to this element *in vitro* (Kang et al., 2009), induced significant luciferase activity in a human insulin promoter episomal construct, and the c.-331C > G mutation suppressed this effect (Student's t test p = 0.02; Figure 6A). Systematic DNA binding site selection studies predict that the C > G mutation impairs GLIS3 binding (Beak et al., 2008), and this was confirmed with electromobility shift assays (Figure S3B). These findings, therefore, indicated that the c.-331C > G mutation disrupts GLIS3 *in vitro* binding to the CC element as well as activation of an episomal *INS* promoter.

Recently, GLIS3 was shown to bind *in vivo* to the *Ins2* promoter, and pancreatic inactivation of *Glis3* in adult mice specifically depletes *Ins2* mRNA in islet cells (Scoville et al., 2019; Yang et al., 2013). To test whether GLIS3 is a direct *in vivo* regulator of the human *INS* gene, we performed ChIP-seq of GLIS3 in human islets. This showed 746 high-confidence binding sites, which displayed marked enrichment of canonical GLIS3 binding sequences, including a *de novo* motif matching the *INS* promoter CC element and a specific binding site in the *INS* promoter (Figures 6B and S4A; Table S2). Additional GLIS3-bound regions were observed in genes known to be important for islet cells, including *PDX1*, *MAFA*, *CREB1*, and *DLL1* (Figure S4B). Furthermore, transduction of two independent short hairpin RNAs (shRNAs) that reduced *GLIS3* mRNA in human EndoCβ-H1 β cells led to ~2-fold lower *INS* mRNA levels (Student's t test p < 0.05; Figure S4C). This provided *in vivo* evidence that GLIS3 is a direct regulator of the human *INS* gene.

To understand GLIS3-mediated regulation of *INS* locus chromatin, we assessed the ability of GLIS3 to activate *INS* in three immortalized non-pancreatic human cell lines in which the *INS* gene is repressed. Combinations of islet cell transcription factors, such as PDX1, MAFA, and NEUROG3 or NEUROD1, have been used to activate β cell programs in pancreatic acinar or liver cells

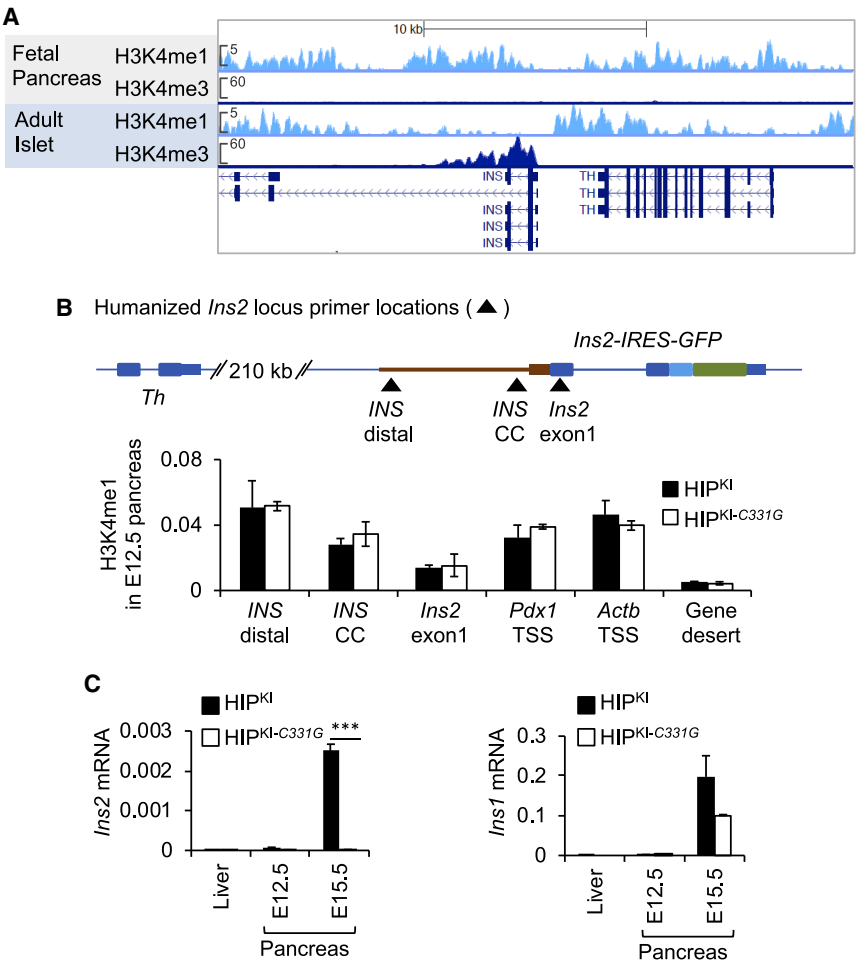

Figure 5. Developmental activation of *INS* promoter chromatin during development

(A) H3K4me1 and H3K4me3 profiles at the *INS* locus showing H3K4me1, but not H3K4me3, enrichment in human fetal pancreas (Carnegie stage 23; Cebola et al., 2015) across the *INS* region and H3K4me3, but not H3K4me1, enrichment in adult human islets (Morán et al., 2012; Pasquali et al., 2014).

(B) Top: approximate location of oligonucleotides for ChIP assays. Bottom: ChIP H3K4me1 enrichments in pancreas from HIP^{KI} or $HIP^{KI\text{-}C331G}$ E12.5 embryos are shown. n = 2 independent experiments from pools of 8–12 embryos. Data are expressed as a percentage of input DNA.

(C) Quantitative PCR analysis for *Ins2* and *Ins1* mRNA from HIP^{KI} or $HIP^{KI\text{-}C331G}$ in E12.5 and E15.5 embryonic pancreas or E15.5 liver (n = 3). Error bars indicate SEM; asterisks indicate Student's t test p values; ***p < 0.0001.

(Yechoor et al., 2009; Zhou et al., 2008), in line with the knowledge that PDX1, MAFA, and NEUROD1 directly bind and regulate the insulin gene promoter in various species (Le Lay and Stein, 2006; Zhao et al., 2005). We found that expression of various combinations of such transcription factors failed to elicit major changes in *INS* mRNA in cell lines from distant lineages, namely HEK293T, MCF7, or SW480 cells (Figures 6C and S5A). By contrast, co-transfection of these factors with GLIS3 led to ectopic activation of the endogenous *INS* gene (Figures 6C and S5A). Other candidate transcription factors that were predicted to bind to the CC element failed to activate *INS* in the presence of PDX1 and NEUROD1 (Figure S5A). Microarray analysis of HEK293T cells transfected with GLIS3, PDX1, NEUROD1, and MAFA showed that *INS* was the most highly induced gene relative to cells that were only transfected with PDX1, MAFA, and NEUROD1 (Figure S5B). These results indicate that GLIS3 has a specific ability to activate the *INS* gene in cell lines from distant lineages, which requires other *INS* promoter-binding transcription factors that do not elicit this effect on their own.

To further understand this unique effect of GLIS3 on the *INS* gene, we examined chromatin accessibility using FAIRE. Misexpression of GLIS3, PDX1, and NEUROD1 created accessible chromatin at the endogenous *INS* gene in HEK293T cells, whereas this was not elicited by PDX1 and NEUROD1 alone (Figure 6D). This effect was direct, as ChIP experiments showed that transfected GLIS3 was bound to the *INS* promoter (Figure S5C). Thus, GLIS3 has a singular ability to bind and activate the *INS* promoter in repressed chromatin cellular environments.

Because GLIS3 activation of episomal INS promoter constructs was impaired by the c.-331C > G mutation, we next tested whether the GLIS3-dependent chromatin pioneering function was also mediated by the CC element. We thus prepared fibroblasts from HIP^{KI} and $HIP^{KI\text{-}C331G}$ embryos. Given that other islet transcription factors are required for the GLIS3 effect, we transduced HIP^{KI} and $HIP^{KI\text{-}C331G}$ mouse embryonic fibroblasts with PDX1, NEUROD1, MAFA, and GLIS3. This combination of transcription factors activated transcription from the humanized locus in HIP fibroblasts, whereas the effect was inhibited by the c.-331C > G mutation (Figure 6E).

These findings, therefore, indicate that GLIS3 has a distinct pioneering function in the activation of human *INS* in an endogenous chromosomal context and indicate that c.-331C > G mutation impairs this function.

DISCUSSION

We have examined the *in vivo* consequences of two gene-regulatory defects that cause diabetes mellitus. We studied an extended cohort of patients with neonatal diabetes and provide firm human genetic evidence that the CC element of the human *INS* gene is selectively vulnerable to loss-of-function mutations. We humanized a large genomic regulatory region in mice and demonstrated that a neonatal diabetes point mutation in this element disrupts an essential pioneering step in the activation of the human *INS* gene. We further demonstrate that GLIS3,

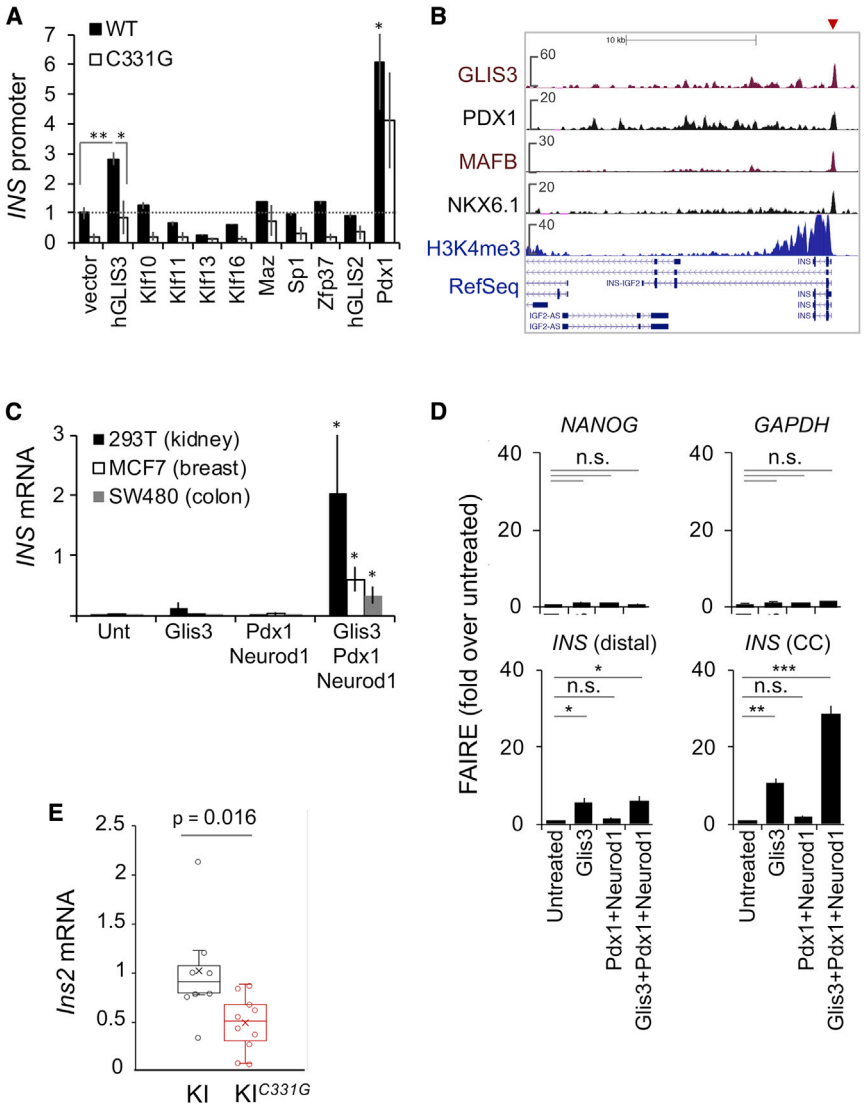

Figure 6. GLIS3 activates the endogenous *INS* gene and requires an intact CC element

(A) Transfection of candidate transcription factors or PDX1 as a positive control, along with *INS* promoter (wild-type or c.-331C > G) luciferase reporter plasmids in ENDOCβ-H1 cells. Statistical comparisons correspond to GLIS3 versus empty expression vectors, both with a wild-type reporter plasmid, or for hGLIS3 vector, the wild-type versus c.-331C > G reporter plasmid.

(B) ChIP-seq shows GLIS3 binding to the *INS* promoter (arrow) in human islets.

(C) GLIS3 activates *INS* in heterologous cell types. HEK293T, MCF7, or SW480 cells were transfected with plasmids encoding indicated transcription factors or left untreated (unt). *INS* mRNA was calculated as *INS* to *GAPDH* mRNA ratios × 1,000. Significance was calculated relative to untreated samples in 3 independent experiments.

(D) FAIRE assessment of accessible chromatin in transfected HEK293T cells. FAIRE DNA was quantified by PCR and expressed as percentage of input DNA and fold enrichment over untreated cells. Statistical significance was calculated relative to untreated samples (n = 3 independent experiments). Expectedly, signal from *NANOG* and *GAPDH* did not change.

(E) GLIS3-dependent activation of *INS* in fibroblasts obtained from HIP^{KI} (n = 7) and $HIP^{KI\text{-}C331G}$ (n = 10) embryos. Fibroblasts were transduced with mouse GLIS3, MAFA, PDX1, and NEUROD1 lentivirus, and RNA was analyzed after 2 days. Two independent experiments were performed with cells from 7 HIP^{KI} and 10 $HIP^{KI\text{-}C331G}$ embryos from two litters. Error bars are SEM; asterisks are Student's t test; *p < 0.05; **p < 0.001; ***p < 0.0001.

which is also mutated in neonatal diabetes and harbors polygenic diabetes risk variants (Barrett et al., 2009; Dupuis et al., 2010; Senée et al., 2006), has a unique role in the activation of *INS* gene chromatin mediated by the CC element that is mutated in neonatal diabetes. These results revealed *cis* and *trans* regulators of an essential mechanism for developmental activation of the endogenous *INS* gene.

Transcriptional regulatory DNA variants play a central role in human disease (Miguel-Escalada et al., 2015), yet so far, most efforts have investigated their function in experimental systems that do not consider their *in vivo* impact (Cannon and Mohlke, 2018; Corradin and Scacheri, 2014; Kircher et al., 2019). This is a major limitation, because it is currently clear that gene regulation entails a complex interplay between elements that are difficult to reproduce outside of an *in vivo* context, including chromatin structure, epigenetic chemical modifications, or noncoding RNAs. Such factors are highly dynamic throughout development and physiological settings. Importantly, *in vitro* models cannot easily examine transcription factor-DNA interactions that overcome repressed chromatin states. Many transcription factors can only bind recognition sequences in accessible DNA, whereas a subset of transcription factors have the ability to bind to nucleosomal-bound DNA and to reprogram silent chromatin (Soufi et al., 2015; Zaret and Carroll, 2011). Such pioneer functions play a major role in differentiation and cellular programming and should thus be studied with *in vivo* approaches that recapitulate salient genomic and chromatin contexts.

Previous work with a trans-species aneuploid model showed that the human chromosome 21 can recapitulate human cell-specific regulatory landscapes in mice (Wilson et al., 2008). Our study has now shown that a human ~3.1-kb genomic region could be integrated into an orthologous region of another mammal and recapitulate stage- and cell-specific functions. Importantly, we have modeled a human noncoding mutation in an extended human regulatory sequence integrated in an orthologous mouse locus, thereby extended earlier models that introduced human mutations in an orthologous mouse sequence (Zhu et al., 2019). This *in vivo* strategy was essential to model CC element mutations, because systematic *in vitro* binding studies and episomal reporter assays have disclosed >16

binding activities and functional elements in the human insulin promoter that do not appear to harbor mutations that are pathogenic in humans (Bonnefond et al., 2011; Docherty et al., 2005; Garin et al., 2010; German et al., 1995; Melloul et al., 2002; Odagiri et al., 1996). Interestingly, a mutation of a 34-bp region that contains the CC element in randomly integrated human *INS* promoter transgenics did not significantly alter promoter activity (Itier et al., 1996). Our humanized model showed that the c.-331C > G mutation did not prevent *INS* chromatin priming in pre-differentiated cells but disrupted H3K4 trimethylation, chromatin accessibility, and transcription factor binding to the *INS* promoter in differentiated β cells. This indicates that the CC element acts as an essential seeding site for chromatin opening and transcriptional activation of the *INS* promoter in β cell development. It also shows that the essential function of this element can only become fully apparent in a natural chromatinized environment, such as that of human patients or mutant HIP mice.

Our studies also show that the Krüppel-like zinc finger protein GLIS3 activates the human *INS* gene *in vivo*. This extends studies showing that GLIS3 binds the mouse *Ins2* promoter *in vivo* and the human *INS* CC element *in vitro* (Kang et al., 2009; ZeRuth et al., 2013). Furthermore, pancreatic *Glis3*-deficient and $Glis3^{+/-}$ mice show severe abnormalities in insulin expression (Scoville et al., 2019; Yang et al., 2013). Importantly, our studies now show that GLIS3 has a selective ability among known *INS* gene regulators to activate *INS* in cellular environments in which this locus is repressed. It is interesting to note that GLIS1, a GLIS3 paralog, has a major impact on reprogramming of pluripotent cells from somatic cells in the presence of other pluripotency transcription factors (Maekawa et al., 2011), and GLIS3 has a similar reprogramming function in some somatic cell lineages (Lee et al., 2017). It is therefore likely that GLIS3 can derepress diverse target genes through combinatorial interactions with cell-specific transcription factors. We have further shown that the c.-331C > G mutation prevented GLIS3-dependent activation of both episomal and integrated human *INS*. These findings, therefore, provide a common mechanism for genetic defects in *GLIS3* and the *INS* CC element.

Our studies, therefore, uncover an unanticipated protagonism of GLIS3 and the CC element of the *INS* promoter to initiate an active chromatin state at the human *INS* gene. Our findings are relevant to understanding genetic mechanisms underlying diabetes, as well as for efforts to use *cis*-acting sequences and transcription factors to activate β cell genes for replacement therapies (Bakhti et al., 2019; Ding et al., 2013; Zhou and Melton, 2018).

STAR★METHODS

Detailed methods are provided in the online version of this paper and include the following:

SUPPLEMENTAL INFORMATION

Supplemental information can be found online at https://doi.org/10.1016/j.celrep.2021.108981.

ACKNOWLEDGMENTS

This research was supported by the Birmingham Fellowship Programme, RD Lawrence Fellowship (Diabetes UK, 20/0006136), and Academy of Medical Sciences Springboard (SBF006\1140) to I.A. Other main funding sources (to J.F.) are Ministerio de Ciencia e Innovación (BFU2014-54284-R and RTI2018-095666-B-I00), Medical Research Council (MR/L02036X/1), a Wellcome Trust Senior Investigator Award (WT101033), European Research Council Advanced Grant (789055), and FP6-LIFESCIHEALTH 518153. E.D.F. is a Diabetes UK RD Lawrence Fellow (19/005971). A.T.H. and S.E. are the recipients of a Wellcome Trust Senior Investigator award (WT098395/Z/12/Z), and A.T.H. is employed as a core member of staff within the NIHR-funded Exeter Clinical Research Facility and is an NIHR senior investigator. S.E.F. has a Sir Henry Dale Fellowship jointly funded by the Wellcome Trust and the Royal Society (105636/Z/14/Z). Human islets for research were supported by the Juvenile Diabetes Research Foundation (2-RSC-2019-724-I-X). Work in CRG was supported by the CERCA Programme, Generalitat de Catalunya, and Centro de Excelencia Severo Ochoa (SEV-2015-0510). CRG acknowledges the support of the Spanish Ministry of Science and Innovation to the EMBL partnership. We thank the University of Barcelona School of Medicine animal facility, Center of Genomic Regulation and Imperial College London Genomics Units, and Larry Chan (Baylor College), Roland Stein (Vanderbilt University), Anton Jetten (NIEHS, NIH, North Carolina), Doris Stoffers (University of Pennsylvania), Jochen Seufert (University of Freiburg), Marko Horb (Marine Biological Laboratory), Alpana Ray (University of Missouri), and Tatsuya Tsurimi (Aichi Cancer Center, Ngoya, Japan) for generous gifts of valuable reagents and Kader Thiam (genOway) for overseeing the design of mouse models. We thank Diego Balboa and Mirabai Cuenca for critical comments on the manuscript. Graphical abstract drawings were by Yasemin Ezel with clipart from Biorender.

AUTHOR CONTRIBUTIONS

I.A. and J.F. conceived and coordinated the study. I.A. performed cell-based and computational studies and supervised mouse analysis. I.A. and M.A.M. performed image analysis of mouse mutants and isolated islets. L.P. purified

human islets. V.G. maintained mouse colonies, G.M. performed SILAC experiments, P.R. designed and created lentiviral vectors, and E.D.F., S.F., S.E., and A.T.H. identified and studied patient mutations. I.A. and J.F. wrote the manuscript with input from the remaining authors.

DECLARATION OF INTERESTS

P.R. is a shareholder and consultant for Endocells/Unicercell Biosolutions. The other authors declare no competing interests.

Received: June 22, 2020
Revised: January 4, 2021
Accepted: March 23, 2021
Published: April 13, 2021

REFERENCES

Akerman, I., Tu, Z., Beucher, A., Rolando, D.M.Y., Sauty-Colace, C., Benazra, M., Nakic, N., Yang, J., Wang, H., Pasquali, L., et al. (2017). Human pancreatic β cell lncRNAs control cell-specific regulatory networks. Cell Metab. *25*, 400–411.

Allen, H.L., Flanagan, S.E., Shaw-Smith, C., De Franco, E., Akerman, I., Caswell, R., Ferrer, J., Hattersley, A.T., and Ellard, S.; International Pancreatic Agenesis Consortium (2011). GATA6 haploinsufficiency causes pancreatic agenesis in humans. Nat. Genet. *44*, 20–22.

Bailey, T.L., Boden, M., Buske, F.A., Frith, M., Grant, C.E., Clementi, L., Ren, J., Li, W.W., and Noble, W.S. (2009). MEME SUITE: tools for motif discovery and searching. Nucleic Acids Res. *37*, W202–W208.

Bakhti, M., Böttcher, A., and Lickert, H. (2019). Modelling the endocrine pancreas in health and disease. Nat. Rev. Endocrinol. *15*, 155–171.

Barrett, J.C., Clayton, D.G., Concannon, P., Akolkar, B., Cooper, J.D., Erlich, H.A., Julier, C., Morahan, G., Nerup, J., Nierras, C., et al.; Type 1 Diabetes Genetics Consortium (2009). Genome-wide association study and meta-analysis find that over 40 loci affect risk of type 1 diabetes. Nat. Genet. *41*, 703–707.

Beak, J.Y., Kang, H.S., Kim, Y.S., and Jetten, A.M. (2008). Functional analysis of the zinc finger and activation domains of Glis3 and mutant Glis3(NDH1). Nucleic Acids Res. *36*, 1690–1702.

Benko, S., Fantes, J.A., Amiel, J., Kleinjan, D.J., Thomas, S., Ramsay, J., Jamshidi, N., Essafi, A., Heaney, S., Gordon, C.T., et al. (2009). Highly conserved non-coding elements on either side of SOX9 associated with Pierre Robin sequence. Nat. Genet. *41*, 359–364.

Biggin, M.D. (2011). Animal transcription networks as highly connected, quantitative continua. Dev. Cell *21*, 611–626.

Bonnefond, A., Lomberk, G., Buttar, N., Busiah, K., Vaillant, E., Lobbens, S., Yengo, L., Dechaume, A., Mignot, B., Simon, A., et al. (2011). Disruption of a novel Kruppel-like transcription factor p300-regulated pathway for insulin biosynthesis revealed by studies of the c.-331 INS mutation found in neonatal diabetes mellitus. J. Biol. Chem. *286*, 28414–28424.

Cannon, M.E., and Mohlke, K.L. (2018). Deciphering the emerging complexities of molecular mechanisms at GWAS loci. Am. J. Hum. Genet. *103*, 637–653.

Cebola, I., Rodríguez-Seguí, S.A., Cho, C.H., Bessa, J., Rovira, M., Luengo, M., Chhatriwala, M., Berry, A., Ponsa-Cobas, J., Maestro, M.A., et al. (2015). TEAD and YAP regulate the enhancer network of human embryonic pancreatic progenitors. Nat. Cell Biol. *17*, 615–626.

Chong, J.X., Buckingham, K.J., Jhangiani, S.N., Boehm, C., Sobreira, N., Smith, J.D., Harrell, T.M., McMillin, M.J., Wiszniewski, W., Gambin, T., et al.; Centers for Mendelian Genomics (2015). The genetic basis of Mendelian phenotypes: discoveries, challenges, and opportunities. Am. J. Hum. Genet. *97*, 199–215.

Corradin, O., and Scacheri, P.C. (2014). Enhancer variants: evaluating functions in common disease. Genome Med. *6*, 85.

Cowper-Sal lari, R., Zhang, X., Wright, J.B., Bailey, S.D., Cole, M.D., Eeckhoute, J., Moore, J.H., and Lupien, M. (2012). Breast cancer risk-associated SNPs modulate the affinity of chromatin for FOXA1 and alter gene expression. Nat. Genet. *44*, 1191–1198.

Creyghton, M.P., Cheng, A.W., Welstead, G.G., Kooistra, T., Carey, B.W., Steine, E.J., Hanna, J., Lodato, M.A., Frampton, G.M., Sharp, P.A., et al. (2010). Histone H3K27ac separates active from poised enhancers and predicts developmental state. Proc. Natl. Acad. Sci. USA *107*, 21931–21936.

Deeb, A., Habeb, A., Kaplan, W., Attia, S., Hadi, S., Osman, A., Al-Jubeh, J., Flanagan, S., DeFranco, E., and Ellard, S. (2016). Genetic characteristics, clinical spectrum, and incidence of neonatal diabetes in the Emirate of AbuDhabi, United Arab Emirates. Am. J. Med. Genet. A. *170*, 602–609.

Demirbilek, H., Arya, V.B., Ozbek, M.N., Houghton, J.A., Baran, R.T., Akar, M., Tekes, S., Tuzun, H., Mackay, D.J., Flanagan, S.E., et al. (2015). Clinical characteristics and molecular genetic analysis of 22 patients with neonatal diabetes from the South-Eastern region of Turkey: predominance of non-KATP channel mutations. Eur. J. Endocrinol. *172*, 697–705.

Ding, L., Gysemans, C., and Mathieu, C. (2013). β-cell differentiation and regeneration in type 1 diabetes. Diabetes Obes. Metab. *15* (*Suppl 3*), 98–104.

Docherty, H.M., Hay, C.W., Ferguson, L.A., Barrow, J., Durward, E., and Docherty, K. (2005). Relative contribution of PDX-1, MafA and E47/beta2 to the regulation of the human insulin promoter. Biochem. J. *389*, 813–820.

Dupuis, J., Langenberg, C., Prokopenko, I., Saxena, R., Soranzo, N., Jackson, A.U., Wheeler, E., Glazer, N.L., Bouatia-Naji, N., Gloyn, A.L., et al.; DIAGRAM Consortium; GIANT Consortium; Global BPgen Consortium; Anders Hamsten on behalf of Procardis Consortium; MAGIC investigators (2010). New genetic loci implicated in fasting glucose homeostasis and their impact on type 2 diabetes risk. Nat. Genet. *42*, 105–116.

Duvillié, B., Cordonnier, N., Deltour, L., Dandoy-Dron, F., Itier, J.M., Monthioux, E., Jami, J., Joshi, R.L., and Bucchini, D. (1997). Phenotypic alterations in insulin-deficient mutant mice. Proc. Natl. Acad. Sci. USA *94*, 5137–5140.

Garin, I., Edghill, E.L., Akerman, I., Rubio-Cabezas, O., Rica, I., Locke, J.M., Maestro, M.A., Alshaikh, A., Bundak, R., del Castillo, G., et al.; Neonatal Diabetes International Group (2010). Recessive mutations in the INS gene result in neonatal diabetes through reduced insulin biosynthesis. Proc. Natl. Acad. Sci. USA *107*, 3105–3110.

Gaulton, K.J., Nammo, T., Pasquali, L., Simon, J.M., Giresi, P.G., Fogarty, M.P., Panhuis, T.M., Mieczkowski, P., Secchi, A., Bosco, D., et al. (2010). A map of open chromatin in human pancreatic islets. Nat. Genet. *42*, 255–259.

German, M., Ashcroft, S., Docherty, K., Edlund, H., Edlund, T., Goodison, S., Imura, H., Kennedy, G., Madsen, O., Melloul, D., et al. (1995). The insulin gene promoter. A simplified nomenclature. Diabetes *44*, 1002–1004.

Hansen, S.K., Párrizas, M., Jensen, M.L., Pruhova, S., Ek, J., Boj, S.F., Johansen, A., Maestro, M.A., Rivera, F., Eiberg, H., et al. (2002). Genetic evidence that HNF-1alpha-dependent transcriptional control of HNF-4alpha is essential for human pancreatic beta cell function. J. Clin. Invest. *110*, 827–833.

Heinz, S., Benner, C., Spann, N., Bertolino, E., Lin, Y.C., Laslo, P., Cheng, J.X., Murre, C., Singh, H., and Glass, C.K. (2010). Simple combinations of lineage-determining transcription factors prime cis-regulatory elements required for macrophage and B cell identities. Mol. Cell *38*, 576–589.

Heinz, S., Romanoski, C.E., Benner, C., Allison, K.A., Kaikkonen, M.U., Orozco, L.D., and Glass, C.K. (2013). Effect of natural genetic variation on enhancer selection and function. Nature *503*, 487–492.

Huang, Y.F., Gulko, B., and Siepel, A. (2017). Fast, scalable prediction of deleterious noncoding variants from functional and population genomic data. Nat. Genet. *49*, 618–624.

Itier, J.M., Douhet, P., Desbois, P., Joshi, R.L., Dandoy-Dron, F., Jami, J., and Bucchini, D. (1996). Human insulin gene expression in transgenic mice: mutational analysis of the regulatory region. Differentiation *60*, 309–316.

Junion, G., Spivakov, M., Girardot, C., Braun, M., Gustafson, E.H., Birney, E., and Furlong, E.E. (2012). A transcription factor collective defines cardiac cell fate and reflects lineage history. Cell *148*, 473–486.

Kang, H.S., Kim, Y.-S., ZeRuth, G., Beak, J.Y., Gerrish, K., Kilic, G., Sosa-Pineda, B., Jensen, J., Pierreux, C.E., Lemaigre, F.P., et al. (2009).

Transcription factor Glis3, a novel critical player in the regulation of pancreatic beta-cell development and insulin gene expression. Mol. Cell. Biol. *29*, 6366–6379.

Kennedy, G.C., German, M.S., and Rutter, W.J. (1995). The minisatellite in the diabetes susceptibility locus IDDM2 regulates insulin transcription. Nat. Genet. *9*, 293–298.

Khoueiry, P., Girardot, C., Ciglar, L., Peng, P.C., Gustafson, E.H., Sinha, S., and Furlong, E.E. (2017). Uncoupling evolutionary changes in DNA sequence, transcription factor occupancy and enhancer activity. eLife *6*, e28440.

Kircher, M., Xiong, C., Martin, B., Schubach, M., Inoue, F., Bell, R.J.A., Costello, J.F., Shendure, J., and Ahituv, N. (2019). Saturation mutagenesis of twenty disease-associated regulatory elements at single base-pair resolution. Nat. Commun. *10*, 3583.

Kowalski, M.H., Qian, H., Hou, Z., Rosen, J.D., Tapia, A.L., Shan, Y., Jain, D., Argos, M., Arnett, D.K., Avery, C., et al.; NHLBI Trans-Omics for Precision Medicine (TOPMed) Consortium; TOPMed Hematology & Hemostasis Working Group (2019). Use of >100,000 NHLBI Trans-Omics for Precision Medicine (TOPMed) Consortium whole genome sequences improves imputation quality and detection of rare variant associations in admixed African and Hispanic/Latino populations. PLoS Genet. *15*, e1008500.

Langmead, B., and Salzberg, S.L. (2012). Fast gapped-read alignment with Bowtie 2. Nat. Methods *9*, 357–359.

Le Lay, J., and Stein, R. (2006). Involvement of PDX-1 in activation of human insulin gene transcription. J. Endocrinol. *188*, 287–294.

Lee, S.Y., Noh, H.B., Kim, H.T., Lee, K.I., and Hwang, D.Y. (2017). Glis family proteins are differentially implicated in the cellular reprogramming of human somatic cells. Oncotarget *8*, 77041–77049.

Leroux, L., Desbois, P., Lamotte, L., Duvillié, B., Cordonnier, N., Jackerott, M., Jami, J., Bucchini, D., and Joshi, R.L. (2001). Compensatory responses in mice carrying a null mutation for Ins1 or Ins2. Diabetes *50* (*Suppl 1*), S150–S153.

Lettice, L.A., Heaney, S.J., Purdie, L.A., Li, L., de Beer, P., Oostra, B.A., Goode, D., Elgar, G., Hill, R.E., and de Graaff, E. (2003). A long-range Shh enhancer regulates expression in the developing limb and fin and is associated with preaxial polydactyly. Hum. Mol. Genet. *12*, 1725–1735.

Maekawa, M., Yamaguchi, K., Nakamura, T., Shibukawa, R., Kodanaka, I., Ichisaka, T., Kawamura, Y., Mochizuki, H., Goshima, N., and Yamanaka, S. (2011). Direct reprogramming of somatic cells is promoted by maternal transcription factor Glis1. Nature *474*, 225–229.

Maestro, M.A., Boj, S.F., Luco, R.F., Pierreux, C.E., Cabedo, J., Servitja, J.M., German, M.S., Rousseau, G.G., Lemaigre, F.P., and Ferrer, J. (2003). Hnf6 and Tcf2 (MODY5) are linked in a gene network operating in a precursor cell domain of the embryonic pancreas. Hum. Mol. Genet. *12*, 3307–3314.

Maurano, M.T., Humbert, R., Rynes, E., Thurman, R.E., Haugen, E., Wang, H., Reynolds, A.P., Sandstrom, R., Qu, H., Brody, J., et al. (2012). Systematic localization of common disease-associated variation in regulatory DNA. Science *337*, 1190–1195.

Melloul, D., Marshak, S., and Cerasi, E. (2002). Regulation of insulin gene transcription. Diabetologia *45*, 309–326.

Miguel-Escalada, I., Pasquali, L., and Ferrer, J. (2015). Transcriptional enhancers: functional insights and role in human disease. Curr. Opin. Genet. Dev. *33*, 71–76.

Mittler, G., Butter, F., and Mann, M. (2009). A SILAC-based DNA protein interaction screen that identifies candidate binding proteins to functional DNA elements. Genome Res. *19*, 284–293.

Miyazaki, J., Araki, K., Yamato, E., Ikegami, H., Asano, T., Shibasaki, Y., Oka, Y., and Yamamura, K. (1990). Establishment of a pancreatic beta cell line that retains glucose-inducible insulin secretion: special reference to expression of glucose transporter isoforms. Endocrinology *127*, 126–132.

Morán, I., Akerman, I., van de Bunt, M., Xie, R., Benazra, M., Nammo, T., Arnes, L., Nakić, N., García-Hurtado, J., Rodríguez-Seguí, S., et al. (2012). Human β cell transcriptome analysis uncovers lncRNAs that are tissue-specific, dynamically regulated, and abnormally expressed in type 2 diabetes. Cell Metab. *16*, 435–448.

Nammo, T., Rodríguez-Seguí, S.A., and Ferrer, J. (2011). Mapping open chromatin with formaldehyde-assisted isolation of regulatory elements. Methods Mol. Biol. *791*, 287–296.

Nano, R., Bosco, D., Kerr-Conte, J.A., Karlsson, M., Charvier, S., Melzi, R., Ezzouaoui, R., Mercalli, A., Hwa, A., Pattou, F., et al. (2015). Human islet distribution programme for basic research: activity over the last 5 years. Diabetologia *58*, 1138–1140.

Odagiri, H., Wang, J., and German, M.S. (1996). Function of the human insulin promoter in primary cultured islet cells. J. Biol. Chem. *271*, 1909–1915.

Párrizas, M., Maestro, M.A., Boj, S.F., Paniagua, A., Casamitjana, R., Gomis, R., Rivera, F., and Ferrer, J. (2001). Hepatic nuclear factor 1-alpha directs nucleosomal hyperacetylation to its tissue-specific transcriptional targets. Mol. Cell. Biol. *21*, 3234–3243.

Pashos, E.E., Park, Y., Wang, X., Raghavan, A., Yang, W., Abbey, D., Peters, D.T., Arbelaez, J., Hernandez, M., Kuperwasser, N., et al. (2017). Large, diverse population cohorts of hiPSCs and derived hepatocyte-like cells reveal functional genetic variation at blood lipid-associated loci. Cell Stem Cell *20*, 558–570.e10.

Pasquali, L., Gaulton, K.J., Rodríguez-Seguí, S.A., Mularoni, L., Miguel-Escalada, I., Akerman, İ., Tena, J.J., Morán, I., Gómez-Marín, C., van de Bunt, M., et al. (2014). Pancreatic islet enhancer clusters enriched in type 2 diabetes risk-associated variants. Nat. Genet. *46*, 136–143.

Scharfmann, R., Pechberty, S., Hazhouz, Y., von Bülow, M., Bricout-Neveu, E., Grenier-Godard, M., Guez, F., Rachdi, L., Lohmann, M., Czernichow, P., and Ravassard, P. (2014). Development of a conditionally immortalized human pancreatic β cell line. J. Clin. Invest. *124*, 2087–2098.

Scoville, D., Lichti-Kaiser, K., Grimm, S., and Jetten, A. (2019). GLIS3 binds pancreatic beta cell regulatory regions alongside other islet transcription factors. J. Endocrinol. Published online July 1, 2019. https://doi.org/10.1530/JOE-19-0182.

Senée, V., Chelala, C., Duchatelet, S., Feng, D., Blanc, H., Cossec, J.C., Charon, C., Nicolino, M., Boileau, P., Cavener, D.R., et al. (2006). Mutations in GLIS3 are responsible for a rare syndrome with neonatal diabetes mellitus and congenital hypothyroidism. Nat. Genet. *38*, 682–687.

Soufi, A., Garcia, M.F., Jaroszewicz, A., Osman, N., Pellegrini, M., and Zaret, K.S. (2015). Pioneer transcription factors target partial DNA motifs on nucleosomes to initiate reprogramming. Cell *161*, 555–568.

van Arensbergen, J., García-Hurtado, J., Moran, I., Maestro, M.A., Xu, X., Van de Casteele, M., Skoudy, A.L., Palassini, M., Heimberg, H., and Ferrer, J. (2010). Derepression of Polycomb targets during pancreatic organogenesis allows insulin-producing beta-cells to adopt a neural gene activity program. Genome Res. *20*, 722–732.

Villar, D., Berthelot, C., Aldridge, S., Rayner, T.F., Lukk, M., Pignatelli, M., Park, T.J., Deaville, R., Erichsen, J.T., Jasinska, A.J., et al. (2015). Enhancer evolution across 20 mammalian species. Cell *160*, 554–566.

Ward, L.D., and Kellis, M. (2012). Interpreting noncoding genetic variation in complex traits and human disease. Nat. Biotechnol. *30*, 1095–1106.

Weedon, M.N., Cebola, I., Patch, A.M., Flanagan, S.E., De Franco, E., Caswell, R., Rodríguez-Seguí, S.A., Shaw-Smith, C., Cho, C.H., Allen, H.L., et al.; International Pancreatic Agenesis Consortium (2014). Recessive mutations in a distal PTF1A enhancer cause isolated pancreatic agenesis. Nat. Genet. *46*, 61–64.

Wilson, M.D., Barbosa-Morais, N.L., Schmidt, D., Conboy, C.M., Vanes, L., Tybulewicz, V.L., Fisher, E.M., Tavaré, S., and Odom, D.T. (2008). Species-specific transcription in mice carrying human chromosome 21. Science *322*, 434–438.

Yang, Y., Chang, B.H., Samson, S.L., Li, M.V., and Chan, L. (2009). The Krüppel-like zinc finger protein Glis3 directly and indirectly activates insulin gene transcription. Nucleic Acids Res. *37*, 2529–2538.

Yang, Y., Chang, B.H., Yechoor, V., Chen, W., Li, L., Tsai, M.J., and Chan, L. (2011). The Krüppel-like zinc finger protein GLIS3 transactivates neurogenin 3 for proper fetal pancreatic islet differentiation in mice. Diabetologia *54*, 2595–2605.

Yang, Y., Chang, B.H., and Chan, L. (2013). Sustained expression of the transcription factor GLIS3 is required for normal beta cell function in adults. EMBO Mol. Med. *5*, 92–104.

Yechoor, V., Liu, V., Espiritu, C., Paul, A., Oka, K., Kojima, H., and Chan, L. (2009). Neurogenin3 is sufficient for transdetermination of hepatic progenitor cells into neo-islets in vivo but not transdifferentiation of hepatocytes. Dev. Cell *16*, 358–373.

Zaret, K.S., and Carroll, J.S. (2011). Pioneer transcription factors: establishing competence for gene expression. Genes Dev. *25*, 2227–2241.

ZeRuth, G.T., Takeda, Y., and Jetten, A.M. (2013). The Krüppel-like protein Gli-similar 3 (Glis3) functions as a key regulator of insulin transcription. Mol. Endocrinol. *27*, 1692–1705.

Zhang, Y., Liu, T., Meyer, C.A., Eeckhoute, J., Johnson, D.S., Bernstein, B.E., Nusbaum, C., Myers, R.M., Brown, M., Li, W., and Liu, X.S. (2008). Model-based analysis of ChIP-Seq (MACS). Genome Biol. *9*, R137.

Zhao, L., Guo, M., Matsuoka, T.A., Hagman, D.K., Parazzoli, S.D., Poitout, V., and Stein, R. (2005). The islet beta cell-enriched MafA activator is a key regulator of insulin gene transcription. J. Biol. Chem. *280*, 11887–11894.

Zhou, Q., and Melton, D.A. (2018). Pancreas regeneration. Nature *557*, 351–358.

Zhou, Q., Brown, J., Kanarek, A., Rajagopal, J., and Melton, D.A. (2008). In vivo reprogramming of adult pancreatic exocrine cells to beta-cells. Nature *455*, 627–632.

Zhu, F., Nair, R.R., Fisher, E.M.C., and Cunningham, T.J. (2019). Humanising the mouse genome piece by piece. Nat. Commun. *10*, 1845.

STAR★METHODS

KEY RESOURCES TABLE

REAGENT or RESOURCE	SOURCE	IDENTIFIER
Antibodies		
GLIS3	Yang et al. (2011); L. Chan lab, Baylor College of Medicine, Texas, USA	PMID 21786021
H3 mono methyl K4	Abcam	ab8895
Histone H3 (acetyl K27)	Abcam	ab4729
H3 tri-methyl K4	Millipore	04-745
FLAG M2 (against GLIS3-FLAG)	Sigma FLAG-M2	F3165
PDX1	BCBC	Ab2027
Insulin	Dako	A0564
gunie pig anti-Glucagon	MilliporeSigma	4031-01F
rabbit anti glucagon	Dako	A0565
Somatostatin	Dako	A0566
GFP	R&D Systems	AF4240
Immunoflourescence secondary antibodies	Jackson immunoResearch	Cy3, Cy5 and Alexa flour 488
Biological samples		
Human Islets	European Consortium on Islet Transplantation (ECIT) AND Islets for Basic Research Program supported by the Juvenile Diabetes Research Foundation	https://ecit.dri-sanraffaele.org and JDRF-program 2-RSC-2019-724-I-X
Chemicals, peptides, and recombinant proteins		
Antibody diluent	DAKO	S3022
β-2-mercaptoethanol	Sigma-Aldrich	M3148-25ML
BSA	Sigma-Aldrich	A3059
BSA (for Endo-C culture only)	Roche	10775835001
Calf Serum	Sigma-Aldrich	C8056-100ML
Collagenase	Roche	11215809103
Diethylaminoethyl (DEAE)	Sigma-Aldrich	67578-5G
DMEM	Lonza	be12-604f
DMEM 5.5mM Glucose	Thermofisher Scientific	31885023
dsDNA BR assay kit	Thermofisher Scientific	Q32853
dsDNA HS assay kit	Thermofisher Scientific	Q32854
ECM gel	Sigma-Aldrich	E1270-10ML
EDTA	Thermofisher Scientific	AM9260G
Ethanol (immunoflourescence)	Panreac Applichem, Spain	141086.1211
Ethanol	Merck Millipore	108543
Fetal Calf Serum (FBS)	Cambrex	14-801/ 91s1810-500
Fibronectin	Sigma-Aldrich	F1141
Formaldehyde	Calbiochem	344198
Glucose	Sigma-Aldrich	G-8270-1KG
Glycine	Sigma-Aldrich	50046-250G
HBSS	Invitrogen	14060-040
HEPES	Sigma-Aldrich	H7523-50G
Histopaque 1077	Sigma-Aldrich	10771-500ml
Histopaque 1119	Sigma-Aldrich	11191-100ml

(*Continued on next page*)

Continued

REAGENT or RESOURCE	SOURCE	IDENTIFIER
L-Glutamine	Cambrex	BE17-605E
LiCl	Sigma-Aldrich	L9650-100G
Lipofectamine 2000	Invitrogen	11668-019
NEBNext Ultra DNA Library Prep Kit	New England Biolabs	E7370L
Newborn calf serum (Endo-C during passage)	GIBCO	16010-159
Nicotinamide	Sigma-aldrich	481907
Normal donkey serum	Jackson Immunoresearch	017-000-121
NP-40 substitute IGEPAL CA-630	Sigma-Aldrich	I8896
Paraformaldehyde	Agar Scientific	R1026
PBS	Sigma-Aldrich	D-8537
Penicillin	Lonza	DE17-602E/ 17-745E
Phenol chloroform	Sigma-Aldrich	77617-100ML
Power SYBR green mastermix	Applied Biosystems	4368702
Protease inhibitor cocktail	Roche	4693132001
Protein A Sepharose beads	Ge Healthcare	17-0780-01
Protein G Sepharose beads	Ge Healthcare	17-0618-01
Proteinase K	Fermentas	EO0492
Qiaquick columns	QIAGEN	28106
RNase A	Sigma-Aldrich	R4875-100MG
RPMI 1640 medium	Lonza	BE12-702F
RPMI 1640 medium- without glucose	Lonza	BE12-752F
SDS	Sigma-Aldrich	71736-500ML
SDS (ChIP)	Invitrogen	15553-027
Sodium selenite	Sigma-Aldrich	S9133
Sodium-chloride	Sigma-Aldrich	S3014
Sodium-deoxycholate	Sigma-Aldrich	30970-100G
Stratagene Site directed mutagenesis kit	Stratagene (currently Thermofisher)	A13282
Streptomycin	Lonza	DE17-602E/ 17-745E
Superscript III Reverse Transcriptase	Invitrogen	18080093
SYBR green mastermix	Applied Biosystems	4368708
TaqMan Probes	Applied Biosystems	costom
Transferrin	Sigma-Aldrich	T8158-100MG
TriPure reagent	Invitrogen/ Roche	11667165001
Tris-HCL	Life Technologies	15568-025
Trypsin-EDTA 0.05%	GIBCO	25300062
Xylene	PanReac/AppliChem	211769.1714
Critical commercial assays		
Dual-LuciferaseReporter Assay System	Promega	E1960
Deposited data		
GLIS3 ChIP-seq in human islets	This paper	GSE151405
H3K4me1, Human fetal pancrease	Cebola et al., 2015	PMID: 25915126
H3K4me3, Human fetal pancrease	Cebola et al., 2015	PMID:25915126
H3K4me1, Human donor-derived islet	Pasquali et al., 2014	PMID:24413736
H3K4me3, Human donor-derived islet	Pasquali et al., 2014	PMID:24413736
H3K27ac, Human donor-derived islet	Pasquali et al., 2014	PMID:24413736
PDX1, Human donor-derived islet	Pasquali et al., 2014	PMID:24413736
NKX6-1, Human donor-derived islet	Pasquali et al., 2014	PMID:24413736
FOXA2, Human donor-derived islet	Pasquali et al., 2014	PMID:24413736

(*Continued on next page*)

Continued		
REAGENT or RESOURCE	SOURCE	IDENTIFIER
MAFB, Human donor-derived islet	Pasquali et al., 2014	PMID:24413736
RNA-seq, Human donor-derived islet	Akerman et al., 2017	PMID:28041957
Experimental models: cell lines		
EndoCβ-H1	Philippe Ravassard Laboratory	N/A
Mouse embryonic fibroblasts (MEFs)	Generated in this study	N/A
HEK293T	ATCC	ATCC CRL-11268
MCF7	ATCC	HTB-22
SW480	ATCC	CCL-228
Experimental models: organisms/strains		
C57BL/6	Charles River	C57BL/6 (inbred)
HIPKI, HIPKI-C331G	Generated in this study	N/A
Oligonucleotides		
Primers used in this study - Table S3	IDT	N/A
Taqman Probe Ins1	Applied Biosystems	Mm01259683_g1
Taqman Probe Ins2	Applied Biosystems	Mm00731595_gh
Taqman Probe INS	Applied Biosystems	Hs02741908_m1
Taqman Probe Actb	Applied Biosystems	Mm00607939_s1
Taqman Probe ACTB	Applied Biosystems	Hs01060665_g1
Software and algorithms		
FASTQC	Babraham institute	https://www.bioinformatics.babraham.ac.uk/projects/fastqc/
Bowtie2	Langmead and Salzberg, 2012	http://bowtie-bio.sourceforge.net/bowtie2/index.shtml
MACS2	Zhang et al., 2008	https://github.com/macs3-project/MACS/wiki/Install-macs2
Picard Suite	Broad Institute	https://broadinstitute.github.io/picard/
Rstudio	RStudio Team (2020). RStudio: Integrated Development for R.	https://www.rstudio.com/

RESOURCE AVAILABILITY

Lead contact

Further information and requests for resources and reagents should be directed to and will be fulfilled by Ildem Akerman (i.akerman@bham.ac.uk).

Materials availability

Materials generated in this study are available upon request from the lead contact.

Data and code availability

Accession number for GLIS3 ChIP-seq data is GEO: GSE151405 (https://www.ncbi.nlm.nih.gov/geo/query/acc.cgi?acc=GSE151405).

All code generated during this study is available upon request.

EXPERIMENTAL MODEL AND SUBJECT DETAILS

Patients with monogenic diabetes

The study was conducted in accordance with the Declaration of Helsinki principles with informed parental consent given on behalf of children. Patients reported in this study comprise all probands and family members with *INS* promoter homozygous or compound heterozygous mutations sequenced in the Exeter Genomics laboratory, and 3 additional patients from the original joint description of recessive *INS* mutations (DM1293.1, DM1293.2 and DM1265 in Table S1). The coding, flanking intronic regions and up to 450 bp

upstream of the *INS* transcriptional start site (NM_000207.2) were analyzed by Sanger sequencing as previously described (Garin et al., 2010). Clinical information was provided by the referring clinicians via a neonatal diabetes request form (available at https://www.diabetesgenes.org) and from clinical notes.

Generation of HIP^{KI} and HIP$^{KI\text{-}C331G}$ mice

Mouse experiments were conducted following procedures approved by the Ethical Committee of Animal Experimentation of the University of Barcelona. Targeted replacement of *Ins2* with human *INS* 5′ flanking sequences driving *Ins2* and GFP was performed as schematized in Figure 1 (genOway). The exact sequences of these regions are provided in File S1. In brief, targeting vectors were generated with a 3.10 kb unmodified or mutated (c.C331G) 5′ flanking *INS* region, *Ins2* exon 1, intron, and exon 2, an IRES-GFP reporter cassette inserted in the 3′ untranslated region of *Ins2* exon 2, followed by a neomycin selection cassette flanked by loxP sites. This construct was flanked by 5.3 kb and 1.8 kb C57BL/6J mouse homology arms. Targeting of this vector was carried out by homologous recombination in C57BL/6J embryonic stem cells, using a diphtheria toxon A cassette for negative selection. Recombinants were verified by PCR screening and Southern blotting. Four suitable clones resulted, which were used for blastocyst injections and generation of the HIP knock-in mouse strains.-This was followed by CRE-mediated excision of the neomycin cassette *in vivo*, and again verified by PCR screening and Southern blotting. The sequence of the replaced region was verified by Sanger sequencing. Oligonucleotides used for genotyping are shown in Table S3.

Human islets

Human pancreatic islets were obtained through the European Consortium on Islet Transplantation (ECIT), Islets for Basic Research Program supported by the Juvenile Diabetes Research Foundation (program 2-RSC-2019-724-I-X). Pancreatic islets were isolated from multiorgan donors without a history of glucose intolerance (Nano et al., 2015), shipped in culture medium and re-cultured at 37°C in a humidified chamber with 5% CO_2 in glucose-free RPMI 1640 supplemented with 10% fetal calf serum, 100 U/ml penicillin, 100 U/ml streptomycin and 11mM glucose for three days before analysis.

EndoCβ-H1 cell line and culture

EndoCβ-H1 cells were obtained from P. Ravassard and cultured on plastic tissue culture vessels coated with 2 μg/ml Fibronectin and 1% extracellular matrix (ECM) (Sigma-Aldrich) and with the following media: DMEM containing 5.5 mM glucose (GIBCO), 2% bovine serum albumin (BSA, Roche), 2 mM glutamine, 10 mM nicotinamide, 100 international units (U)/ml penicillin, 100 μg/ml streptomycin (P/S), 50 μM β-2-mercaptoethanol, 5.5 μg/ml transferrin and 6.6 ng/ml sodium selenite at 37°C in a humidified chamber with 5% CO_2.

MEF, HEK293T, MCF7 and SW480 cultures and cell lines

Mouse embryonic fibroblasts (MEFs) were obtained from E15.5 HIP^{KI} and HIP$^{KI\text{-}C331G}$ mouse embryos by clipping the tail tips and culturing in media (DMEM (with glucose) supplemented with 10% fetal calf serum, 100 U/ml penicillin, 100 U/ml streptomycin at 37°C in a humidified chamber with 5% CO2). HIP^{KI} and HIP$^{KI\text{-}C331G}$ MEFs, HEK293T, MCF7 and SW480 cells were maintained in DMEM (Lonza) and supplemented with 10% fetal calf serum, 100 U/ml penicillin, 100 U/ml streptomycin at 37°C in a humidified chamber with 5% CO2.

METHOD DETAILS

Immunofluorescence

Pancreases were processed for immunofluorescence as previously described (Maestro et al., 2003).Tissues were fixed in 4% paraformaldehyde-PBS overnight at 4°C with gentle rotation, then washed once in 20 mL cold PBS and embedded in parrafin. Paraffin blocks were cut into 4 μm sections, deparaffinized with xylene by washing twice with a 15 minutes incubation. Xylene was removed and the blocks were rehydrated through serial washes with 5 mL ethanol-water (100% Ethanol incubated for 5 min; 95% Ethanol incubated for 5 min; 75% Ethanol incubated for 5 min; 100% Water incubated for 5 min) followed by an incubation with PBS for 5 min. Sections were blocked for 30 min at room temperature in antibody diluent (DAKO Corporation) with 3% normal serum-PBS solution, using serum from the same species as the secondary antibody, and incubated overnight at 4°C with primary antibodies diluted in 100 μL of blocking buffer per section. Antibody dilutions used were: anti-insulin 1:200, anti somatostatin 1:200, rabbit anti glucagon 1:200, guinea pig anti glucagon 1:1000, anti-GFP 1:200. We then incubated one hour at room temperature with secondary antibodies also diluted in blocking buffer (100 μl/section) at the manufacturer's recommended concentration (1:400 for fluorochromes Cy3 and Cy5 and 1:800 for Alexa 488 fluorochrome). Images were acquired using Leica TSE confocal microscope for immunofluorescence. Antibodies used are shown in Table S3.

Mouse islets and embryonic pancreas isolation and processing

Mouse islets were isolated using previously described protocols (Párrizas et al., 2001; van Arensbergen et al., 2010). C57BL/6, HIP^{KI} or HIP$^{KI\text{-}C331G}$ mice were anesthetized with urethane (15% solution, 1 ml/kg) and sacrificed. Pancreatic islets were isolated using the following procedure: a cannula tube was inserted in the main pancreatic duct and the pancreas was inflated with Hanks' balanced salt solution (HBSS) buffer freshly added with 3U Collagenase P per ml. The pancreas was then removed, placed in a 15 mL falcon

tube and digested for 10 min at 37°C in a water bath with constant, gentle agitation. The cell suspension was washed twice in 15 mL cold HBSS–0.5% bovine serum albumin (HBSS-BSA), resuspended in 5 mL cold HBSS–BSA and gently passed through a needle (0.8 mm diameter, 25 mm gauge). Islets were then washed by adding 10 mL of HBSS-BSA and sedimented for 3 minutes followed by removal of 10 mL from the top half of the solution (islets sediment to the bottom 5 ml). Wash procedure was repeated 3 times. Islets were then sedimented at 1800 rpm (580 g) for 1 min at 4°C and supernatant was removed. Islets were resuspended in 7 mL of HBSS-BSA and gently placed on top of 7 mL of histopaque mixture. Histopaque mixture is made freshly by mixing a 7:3 ratio of Histopaque 1077 and Histopaque 1119 (Sigma Aldrich). Histopaque mixture is heavier than HBSS-BSA and thus two distinct layers are formed. The islets were collected at the interphase of the two layers through centrifugation at 2300 rpm (950 g) for 20 min at room temperature (Acceleration = 5, Deceleration = 0). The islet-enriched fraction was aspirated from the interface, washed three times in cold HBSS–0.5% BSA, and further purified by handpicking under a stereomicroscope. Isolated islets were incubated in 11 mM glucose RPMI 1640 medium, supplemented with 10% fetal calf serum, 100 U/ml penicillin, and 100 U/ml streptomycin at 37°C in a humidified chamber with 5% CO_2 for 48 hours after isolation. For ChIP experiments, mouse islets were immediately crosslinked with formaldehyde after isolation and snap frozen at −80°C until use.

For isolation of embryonic tissue, embryos from timed-pregnancies were placed in cold PBS and dissected under the microscope. Entire embryonic pancreas or liver tissue was removed and placed in 1 mL Tripure (Invitrogen) reagent for RNA harvest.

FAIRE, ChIP and ChIP-Seq

ChIP, ChIP-seq (Chromatin Immunoprecipitation and sequencing) and FAIRE (Formaldehyde-Assisted Isolation of Regulatory Elements) were performed essentially as previously published protocols (Gaulton et al., 2010; Nammo et al., 2011; Pasquali et al., 2014). ChIP experiments using antibodies against H3K4me1 and H3K4me3 were performed on ~250 mouse islet equivalents (IEQ) per sample, while ChIP experiments using antibodies against PDX1 were performed on ~400 mouse IEQ per sample. FAIRE experiments were performed on ~250 mouse IEQ. GLIS3 ChiP-seq experiments were performed with ~3000 human IEQ, using a previously described antibody (Yang et al., 2011; Table S3).

For ChIP, all cells were fixed in 1% formaldehyde-PBS for 10 minutes at room temperature with gentle agitation. Fixation was stopped with addition of glycine to a final concentration of 125 mM for 5 minutes with gentle agitation. Fixed cells were washed twice in cold PBS. Fixed islets were then suspended in sonication buffer and sonicated using Bioruptor (Diagenode) to a length of 200–1000 bp (~12 minutes, 45sec ON, 45 s OFF). Samples were diluted with dilution buffer (1:4 ratio) to obtain 1% Triton X-100, 0.1% SDS and 130 mM NaCl and were precleared with high speed spin (12,000 *rcf.*, 5 minutes) followed by incubation with protein A+G-Sepharose beads (1:1) (20 μl/sample) for 2 hours at 4°C. Input DNA (1% of volume of sample) was collected and frozen. Samples were then subjected to immunoprecipitation with the indicated antibodies (1 μL of H3K4me1/3 and PDX1 and 3 μL of GLIS3 antibodies, Antibody sources are provided in Table S3) overnight at 4°C with gentle rotation. Immune-complexes were collected by incubation with protein A or G-Sepharose (15 μl/sample) for 2 h at 4°C with gentle rotation. Beads were washed using standard ChIP wash buffers (1x 1 mL low salt wash buffer, 1x 1 mL high salt wash buffer, 1x 1 mL LiCl buffer, 3x 1 mL TE buffer) and immunocomplexes eluted with 300 μL elution buffer (incubation at room temperature for 15 minutes with gentle agitation). Input and eluted ChIP DNAs were subjected to reverse cross-linking (65°C for 12 hours), RNase A (20 μg) and Proteinase K digestion (90 μg), and purification with Qiaquick columns (QIAGEN).

For FAIRE assays, sonicated chromatin was subjected to phenol chloroform extraction (2x) without immunoprecipitation and wash steps[62,63].

ChIP Buffers

Sonication Buffer: (2% Triton X-100, 0.5 % SDS, 100 mM NaCl, 1 mM EDTA,10 mM Tris-HCl pH 8.0 and 1x protease inhibitor cocktail (freshly added)

Dilution Buffer: 0.75 % Triton X-100, 140 mM NaCl, 1 mM EDTA, 0.1% Na-deoxycholate, 50 mM HEPES pH8.0, 1x protease inhibitor cocktail (freshly added)

Low Salt Wash Buffer: 20 mM Tris-HCl, pH 8.0, 140mM NaCl, 1mM EDTA, 1% Triton X-100, 0.1% Na Deoxycholate, 0.1% SDS, 1x protease inhibitor cocktail (freshly added)

High Salt Wash Buffer: 20 mM Tris-HCl, pH 8.0, 500mM NaCl, 1mM EDTA, 1% Triton X-100, 0.1% Na Deoxycholate, 0.1% SDS, 1x protease inhibitor cocktail (freshly added)

LiCl Buffer: 20mM Tris-HCl (pH 8.0), 250mM LiCl, 1mM EDTA, 0.5% Na Deoxycholate, 0.5% NP-40 substitute (IGEPAL), 1x protease inhibitor cocktail (freshly added)

TE Buffer: 10mM Tris-HCl (pH 8.0), 1mM EDTA, 1x protease inhibitor cocktail (freshly added)

Elution Buffer: 10mM Tris-HCl (pH 8.0), 1mM EDTA, 1% SDS, 1x protease inhibitor cocktail (freshly

ChIP and FAIRE Library Preparation and sequencing

Sequencing and processing were performed as described (Pasquali et al., 2014). Input DNA samples were quantified with QUBIT dsDNA BR assay kit (Q32853), and ChIP DNA samples were quantified with QUBIT dsDNA HS assay kit (Q32854). Quantitation

was performed using Qubit 2.0 fluorometer. ChIP-Seq DNA libraries were prepared from 5-10 ng of Input DNA or ChIP DNA using NEBNext Ultra DNA Library Prep Kit for Illumina sequencing (New England BioLabs, # E7370L) by the Imperial College Genomics Facility. Libraries were sequenced using Illumina HiSeq2500.

ChIP and FAIRE data analysis

Reads were subjected to quality control analysis using FastQC (v0.11.5) followed by trimming by the Picard suite (default options). Trimmed reads were aligned to the human genome (hg19) using bowtie (Langmead and Salzberg, 2012) (v2.2.6, default options). Peaks were called using MACS2 (Zhang et al., 2008) (v2.2.1, q-value cutoff 0.05, band width 300) as enrichment over ChIP Input DNA. GLIS3-bound regions (peaks) are provided in Table S2.

References for new and previously reported human islet and fetal pancreas ChIP-seq datasets used in this study (Cebola et al., 2015; Morán et al., 2012; Pasquali et al., 2014) are provided in Table S4.

Quantitative PCR analysis

RNA was isolated using TriPure reagent as described (Akerman et al., 2017) following manufacturer's instructions. RNA quality was ascertained with a 2100 Agilent Bioanalyzer (RIN > 8). Ins2, INS, ActB and Ins2 intronic transcripts were measured using TaqMan (Applied Biosystems) probes, while other regions were quantified using oligonucleotide primers and SYBR green mastermix (Illumina). cDNA synthesis was carried out using Superscript III (Invitrogen) and real-time PCR was performed with the ABI 7300 Real Time PCR system using the Power SYBR Green reagent (Applied Biosystems). Serial dilutions of genomic DNA (5 data points) were used to establish a standard curve. SDS software (Applied Biosystems) was used to generate quantitative values based on the standard curve with arbitrary units. All mRNA levels were normalized to ActB or Hprt as indicated in Figure legends. Oligonucleotides and TaqMan probe sequences can be found in Table S3.

In silico motif analysis

To identify candidate transcription factors that bind the CC element, we performed *in silico* motif searches using the MEME suite (Bailey et al., 2009) using the normal and mutated (c.331 C > G) sequences. Analysis of *de novo* and previously characterized position weight matrixes (PWM) was performed with HOMER (v3.12) (Heinz et al., 2010) using peak summit coordinates and flags -size −50,50 -len 6,8,10,12.

GLIS3 knockdown in EndoCβ-H1 cells

Lentiviral-mediated knockdown of GLIS3 in the human pancreatic β-cell line EndoCβ-H1 was performed with two independent shRNAs placed in artificial miRNAs as described in detail (Akerman et al., 2017). In brief, five non-targeting and two GLIS3-targeting amiRNAs were designed using BLOCK-IT software (Invitrogen) and cloned into pTRIP-CMV gateway vectors as described (Akerman et al., 2017). These were then used to produce lentiviruses (Scharfmann et al., 2014), which were transduced into the EndoC-βH1 cells. For knockdown experiments, cells were dissociated with trypsin (0.05%), washed twice with room temperature PBS. 10^5 cells per well (24 wells) were incubated with lentivirus (60 ng of p24 capsid protein) and 10μg/ ml Diethylaminoethyl (DEAE) in 400 μL of medium for 1 hour at 37°C. Cells were harvested at 80 hours post-transduction, and RNA levels were assessed using real time PCR. The efficiency of transduction was judged to be > 95% based on GFP expression. Oligonucleotides used for shRNAs are shown in Table S3.

Luciferase assays

INS promoter activity was measured by transfection of a reporter plasmid: pSOUAPRL-251hINS-Luc (Roland Stein, Vanderbilt University), which contains 251 bp of human *INS* proximal promoter DNA located in front of the Firefly luciferase cDNA. The c.C331G mutation was introduced using site directed mutagenesis (Garin et al., 2010) using Stratagene site directed mutagenesis kit, following manufacturer's instructions. The presence of the mutation was verified by Sanger sequencing. The plasmids (0.5 μg/24 well) were transfected into EndoCβ-H1 with Lipofectamine 2000 at 4:1 luciferase:overexpression vector ratio as previously described (Allen et al., 2011), following manufacturer's instructions. We co-transfected a Renilla expressing construct (pGL4.75, 0.02 ng) as a normalizer to correct for differences in transfection efficiency. Expression vectors used in co-transfections are given in Table S3. Luciferase activity was measured at 48 hours post- transfection using a luminometer (Promega Veritas Microplate luminometer) with the reagents of the Promega Dual-Luciferase Reporter Assay System.

Activation of endogenous INS in heterologous cell types

MEFs were transduced with lentiviral vectors, one encoding the transcription factors PDX1, NEUROD1 and MAFA in a polycistronic transcript, and the other mouse GLIS3-ΔN155 (Beak et al., 2008; Table S3). Cells were harvested 48 hours post transduction and subjected to quantitative PCR analysis. HEK293T, MCF7 and SW480 cells were transfected using Lipofectamine 2000, following manufacturer's instructions. We note that the omission of MAFA or substitution of NEUROD1 with NEUROG3 in such experiments resulted in similar *INS* induction levels. For microarray hybridization experiments described in Figure S5, harvested RNA was hybridized to Gene ST 1.0 Affymetrix arrays and the data was analyzed on Affymetrix TAC (v1.0.24) software as described (Pasquali et al., 2014).

SILAC

We used Stable Isotope Labeling by Amino acids in Cell culture (SILAC) for mass spectrometry identification of proteins that specifically bound to unmodified or mutated (c.C331G) double stranded oligonucleotides containing a 5′ linker and PstI restriction site (Table S3), exactly as described in detail (Mittler et al., 2009), using MIN6 immortalized mouse beta-cells (Miyazaki et al., 1990). MIN6 cells were maintained in DMEM (4.5g/L Glucose), 15% fetal calf serum, 100 U/ml penicillin, 100 U/ml streptomycin at 37°C in a humidified chamber with 5% CO2) and 50 μM beta-mercaptoethanol. SILAC identified 4 proteins whose binding was affected by the mutation: Krueppel-like factor 13 (UniProtKB/Swiss-Prot Q9Y2Y9), Krueppel-like factor 16 (UniProtKB/Swiss-Prot Q9BXK1), MAZ (UniProtKB/TrEMBL Q8IUI2) and ZFP37 (UniProtKB/Swiss-Prot Q9Y6Q3).

QUANTIFICATION AND STATISTICAL ANALYSIS

Boxplots were drawn using Rstudio (v3.5). Line within the boxplot represents median, whereas the bounds of the box define the first and third quartiles. Bottom and top of whiskers represent minimum and maximum numbers respectively for each boxplot. Dot plots and bar plots were drawn using Excel. Where indicated, Student's t test was used to calculate statistically significant differences between samples.

Cell Reports, Volume *35*

Supplemental information

Neonatal diabetes mutations disrupt a chromatin pioneering function that activates the human insulin gene

Ildem Akerman, Miguel Angel Maestro, Elisa De Franco, Vanessa Grau, Sarah Flanagan, Javier García-Hurtado, Gerhard Mittler, Philippe Ravassard, Lorenzo Piemonti, Sian Ellard, Andrew T. Hattersley, and Jorge Ferrer

Figure S1

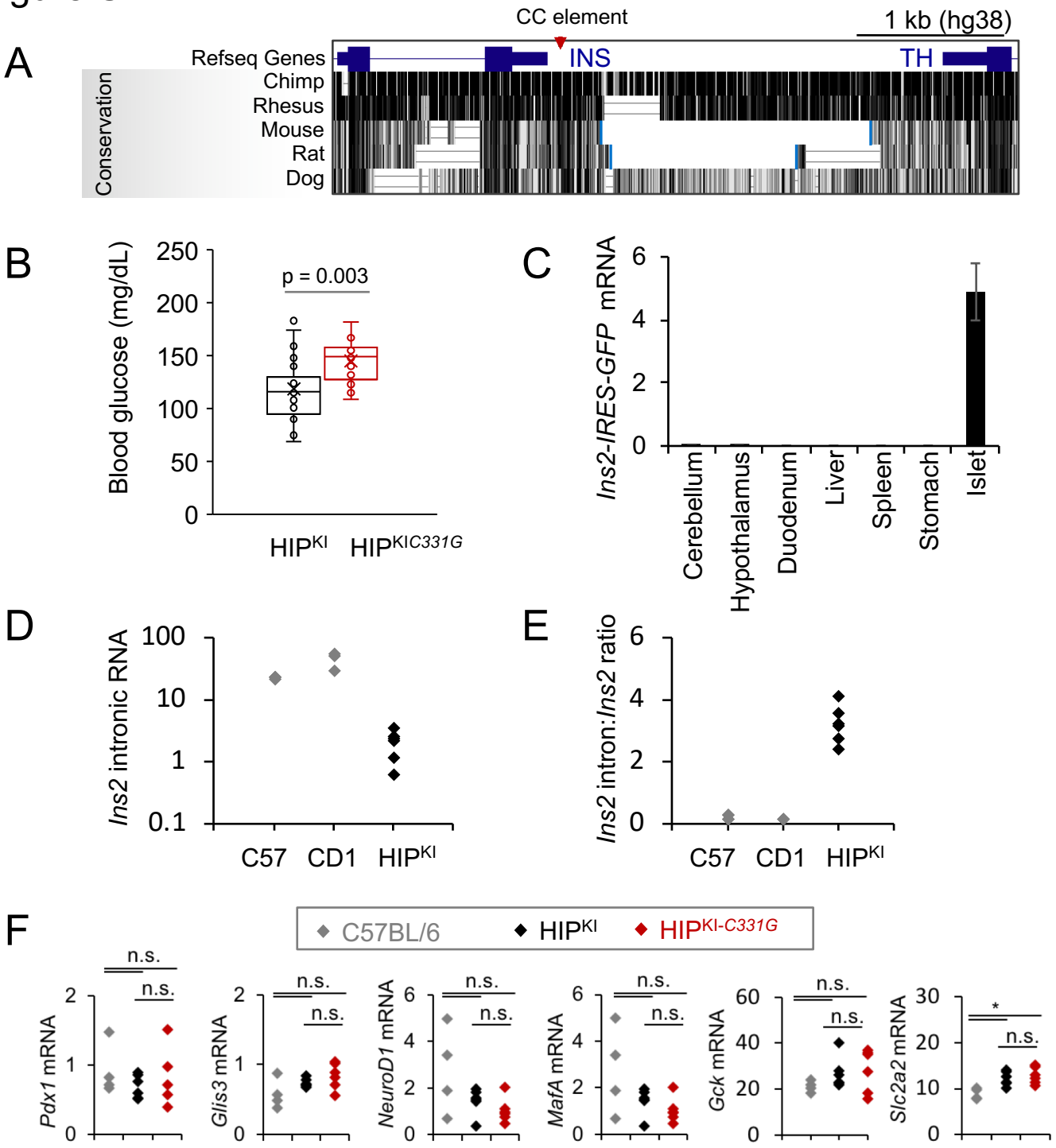

Figure S1. Related to Main Figure 1

(A) UCSC genome browser snapshot of the region between the INS gene and the TH gene. Multiz Alignment representing the level of conservation between the displayed species is shown.

(B) Glycemia from *ad libitum*-fed HIP^{KI} and HIP$^{KI\text{-}C331G}$ mice. P values were calculated with Student's t test.

(C) Quantification of *Ins2-IRES-GFP* mRNA in islets and a panel of tissues in HIP^{KI} mice. Bars represent average values normalised to Actb mRNA from n=6 mice. Cerebellum and hypothalamus display ~50,000 and ~850,000 fold less Ins2-IRES-GFP mRNA respectively, while no transcription is detectable in other tissues.

(D) Measurements of intronic Ins2 transcript levels. Ins2 intronic transcripts, representing the amount of nascent transcription, was quantified using quantitative PCR with taqman probes in islets isolated from C57BL/6 mice (n=4) or HIPKI (n=6).

(E) Nascent and spliced Ins2 RNA ratios in wild type and HIP^{KI} mice. Intronic Ins2 transcript levels and Ins2 transcript levels were quantified using taqman probes in islets isolated from C57BL/6 mice (n=4) or HIP^{KI} (n=6).

(F) Reverse transcription quantitative PCR for *Pdx1, Glis3, NeuroD1, and MafA* mRNAs from pancreatic islets from 3-5 month control C57BL/6 (n=4), HIP^{KI} (n=6) and HIP$^{KI\text{-}C331G}$ (n=6) mice. Values were normalized to *Actb* or *Hprt* mRNAs. (*) Asterisk indicate significance <0.05 by ANOVA unpaired t=test.

Figure S2

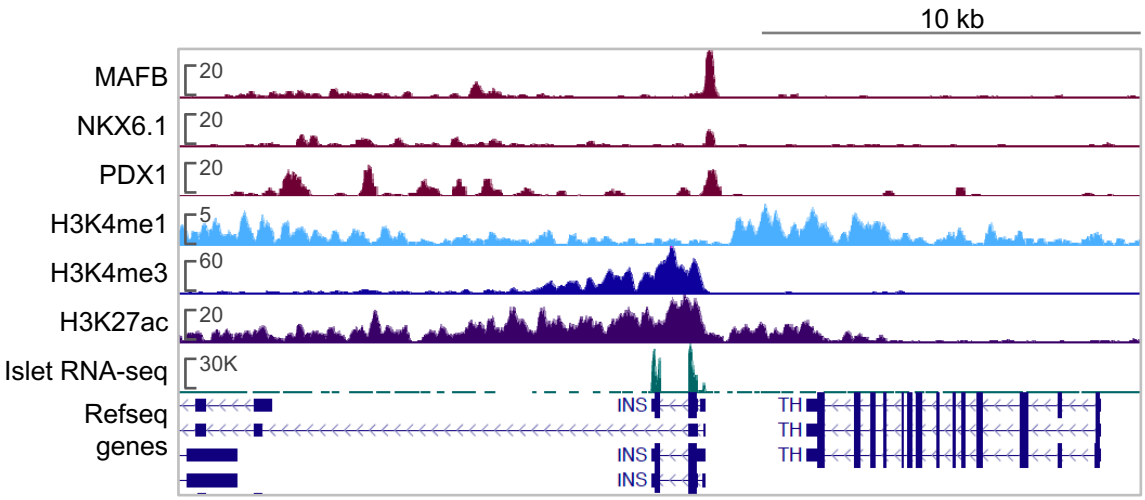

Figure S2. Related to Main Figure 4.
Chromatin landscape of the human *INS* locus in human pancreatic islets. ChIP-seq profiles of activating histone marks H3K4 trimethylation and H3K27 acetylation[12]. All scales represent RPKMs.

Figure S3

A

Transcription factor	Identification method	Activation of wild type *INS* in episomal assay	Activation of endogenous *INS*
Klf13	SILAC	-	-
Klf16	SILAC	-	-
Maz (PUR1)	SILAC	-	-
Zfp37	SILAC	-	-
SP1	in silico motif search	-	na
Glis2	Literature (PMID:21127075)	-	-
Glis3	Literature (PMID:23927931, 19264802)	+	+
Klf10	In silico motif search	-	-
Klf11	Literature (PMID:21592955, 21592955)	-	-

B

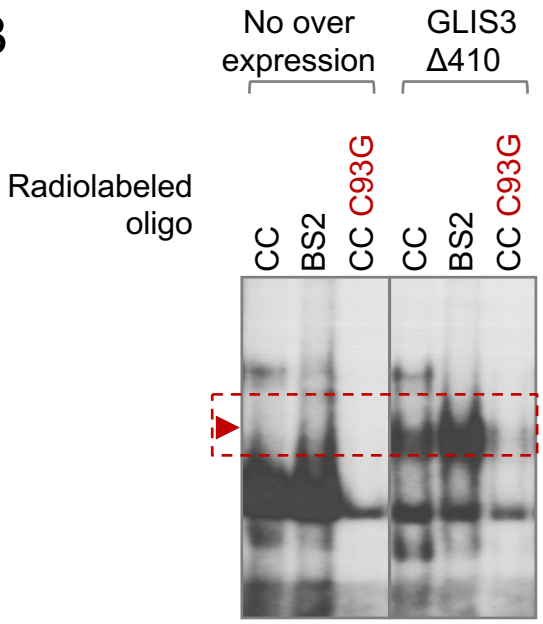

Figure S3. Related to Main Figure 6
(A) Candidate DNA-binding transcription factor regulators of the *INS* gene that underlie the deleterious effects of the c.-331C>G mutation. Four transcription factors were selected based on differential binding to c.-331C vs. c.-331C>G double stranded oligonucleotides in SILAC experiments in MIN6 b cells, while others were selected based on *in silico* predicted differential binding to c.-331C vs. c.-331C>G *INS* sequences or published studies from indicated references. The summary table emphasizes that amongst these candidates only GLIS3 led to activation of the unmodified episomal insulin promoter plasmid, and activated *INS* mRNA in non-pancreatic cell lines in the presence of islet transcription factors as shown in Figure S5.
(B) Electromobility shift assays (EMSA) from HEK 293T cells transfected with human GLIS3Δ410 cDNA show binding to CC element oligonucleotides and BS2, another previously reported GLIS3 recognition sequence in the INS 5' flanking regions[29], but not to the CC element carrying the -331C>G mutation.

Figure S4

A

Top PWMs for known TFs

Sequence motif	Name	p-value	% of Targets Sequences with Motif	% of Background Sequences with Motif
	**GLIS3**(Zf)/Thyroid-Glis3.GFP-ChIP-Seq(GSE103297)	1e-52	38.18%	15.21%
	**Zic3**(Zf)/mES-Zic3-ChIP-Seq(GSE37889)	1e-27	15.62%	4.86%
	Unknown-ESC-element/mES-Nanog-ChIP-Seq(GSE11724)	1e-18	10.95%	3.53%

De novo enriched motif

p-value:	1.00E-15
% of Target Sequences with motif	18.29%
% of Background Sequences with motif	8.68%

B

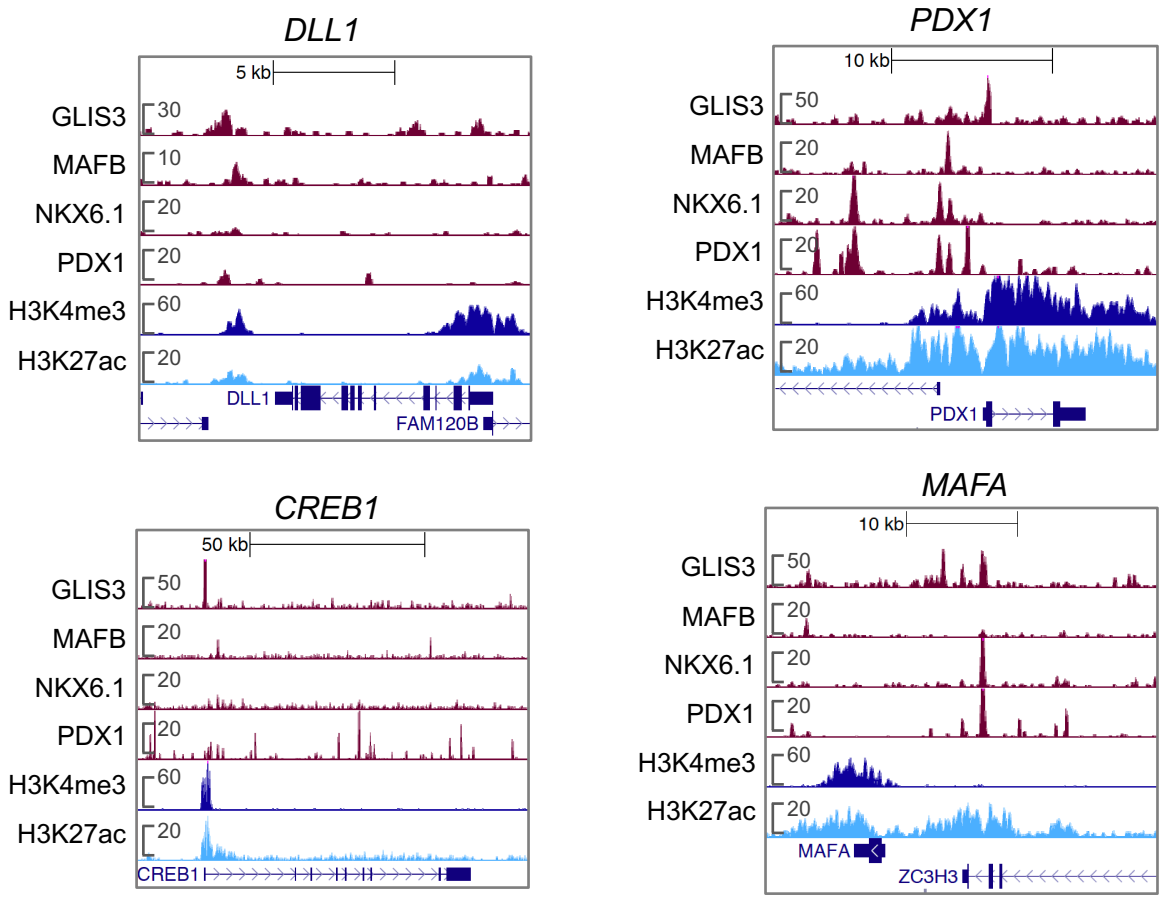

C

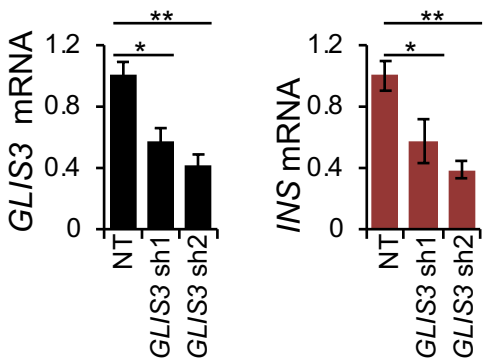

Figure S4. Related to Main Figure 6

(A) The three most enriched position weight matrixes (PWMs) at GLIS3-bound regions in human islets included a previously identified GLIS3-bound PWM (left panel). Discovery of *de novo* enriched PWMs identified sequence PWMs matching known GLIS3 recognition sequences, including one matching the *INS* CC element (right panel).

(B) Examples of GLIS3-bound regions in human pancreatic islets at selected loci, along with binding profiles of other human pancreatic islet transcription factors.

(C) Quantitative reverse-transcription PCR of INS and GLIS3 mRNAs after lentiviral-mediated knockdown of GLIS3, using two independent shRNA sequences, in EndoCb-H1 human b-cells. Student's t-test * $p < 0.05$ or ** $p < 0.001$.

Figure S5

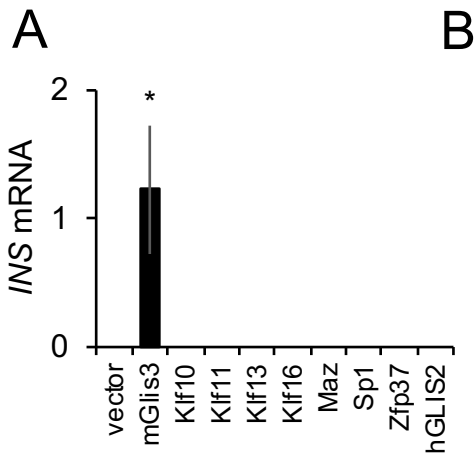

B

Gene Symbol	Gene Title	PNM* vs Unt (Fold Change)	Glis3+ PNM* vs Unt (Fold Change)
INS	*insulin*	*1.03*	*4.54*
MAP2K5	mitogen-activated protein kinase kinase5	3.78	3.42
DLL1	delta-like 1 (Drosophila)	2.02	3.36
NKX2-2	NK2 homeobox 2	2.03	3.21
ATOH7	atonal homolog 7 (Drosophila)	2.45	3.00
CDKN1C	cyclin-dependent kinase inhibitor1C	1.37	2.96
SECTM1	secreted and transmembrane 1	1.32	2.88
C8orf47	chromosome8 open reading frame47	2.36	2.85
EDNRB	endothelin receptor type B	1.87	2.83

*PNM = PDX1, MAFA, NEUROD1

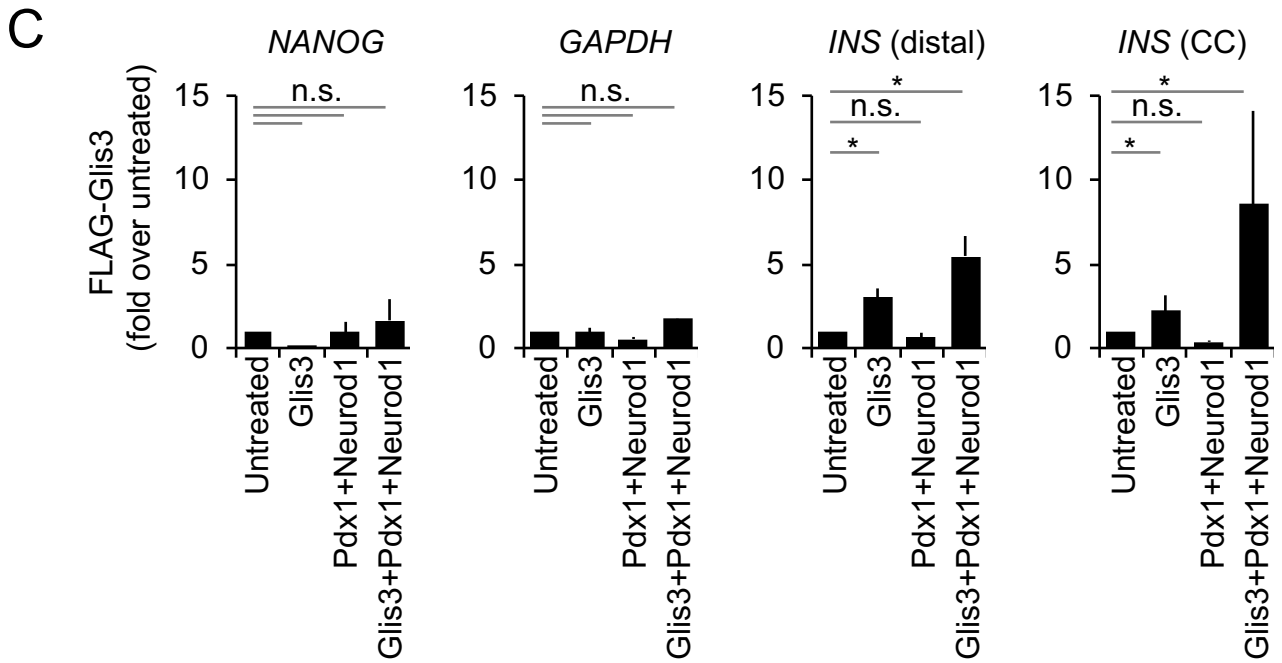

Figure S5. Related to Main Figure 6

(A) GLIS3, but not other candidate transcription factors that bind CC, activate *INS* in a heterologous cell type. HEK 293T cells were either left untreated (Unt) or transfected with plasmids overexpressing the indicated transcription factors along with NEUROD1 and PDX1. *INS* mRNA are *INS* to *GAPDH* mRNA ratios X 1000. Statistical significance was calculated relative to untreated samples (n = 3 independent experiments). * Student's t-test, $p < 0.05$. Analogous experiments were performed in the presence of MAFA, or NEUROG3 instead of NEUROD1, yielding similar results.

(B) Table showing the list of genes most impacted by the overexpression of GLIS3+ PNM (PDX1, NEUROD1, MAFA) vs. PNM alone, in HEK 293T cells. Cells were either left untreated or transfected with the indicated transcription factors. At 3 days post transfection, RNA was quantified using microarrays. Values indicate fold-difference in expression relative to control cells. This experiment was performed with a single replicate and provides an unbiased confirmation that *INS* was the single most induced gene when GLIS3 was added to the transcription factor cocktail.

(C) ChIP of FLAG-tagged GLIS3 in HEK 293T cells transfected with the indicated transcription factors. ChIP DNA was quantified by RT-PCR and expressed as percentage of input DNA and as fold enrichment over untreated HEK 293T cells. Statistical significance was calculated relative to untreated (Unt) samples using Student's t-test (n=3 experiments). As expected, *NANOG* promoter and *GAPDH* enhancer showed no changes between treatments.